



This is to certify that the

# thesis entitled A VISCOUS DIFFUSION MODEL FOR VORTEX-IN-CELL CALCULATIONS

presented by

Kue Pan

has been accepted towards fulfillment of the requirements for

MASTER OF SCIENCE degree in MECHANICAL ENGINERRING

Major professor

Date 2/21/86

O-7639

MSU is an Affirmative Action/Equal Opportunity Institution



RETURNING MATERIALS:
Place in book drop to remove this checkout from your record. FINES will be charged if book is returned after the date stamped below.

# A VISCOUS DIFFUSION MODEL FOR VORTEX-IN-CELL CALCULATIONS

By

Kue Pan

#### A THESIS

Submitted to
Michigan State University
in partial fulfillment of the requirements
for degree of

MASTER OF SCIENCE

Department of Mechanical Engineering

#### ABSTRACT

# A VISCOUS DIFFUSION MODEL FOR VORTEX-IN-CELL CALCULATIONS

Вy

#### Kue Pan

A Vortex-In-Cell technique has been used to study various vortex ring evolutions in two dimensions. The molecular diffusion process is modeled by using a combination of a modified vorticity gradient approximation with a nine-grid-point, conservative redistribution filter. To examine the accuracy and reliability of the algorithm, both one and two-dimensional test cases were investigated. Results are compared with theoretical solutions. Furthermore, the capability to simulate the vortex ring/moving wall interactions with this technique is evaluated by comparing the calculated outcomes with experimental results via stability maps quantitatively and flow visualizations qualitatively. A discussion of the no-slip boundary condition is also included.

To

My Parents

#### **ACKNOWLEDGEMENTS**

I would like to express my great appreciation to my parents for their support during my educational career. Thank you.

I would like to thank my major professor, Dr. Richard W. Bartholomew, for his guidance and generous assistance throughout this research program. I also gratefully acknowledge the other members on my thesis committee, Professor R. E. Falco and Professor C. Y. Wang, for their fruitful discussions and advice. In addition, I wish to thank Miss M. Cline, Mr. C. Chu and Mr. J. Chang for help and friendship they have provided. Thanks are also due Linea, my wife, who gave me a son, Tim, during this study.

# TABLE OF CONTENTS

	Page					
LIST OF TABLES	•					
LIST OF FIGURES						
NOMENCLATURE i						
CHAPTER						
1 INTRODUCTION	1					
2 THE THEORY	7					
2.1 Governing Formulation for Inviscid Fluids	7					
2.2 Viscous Diffusion Model	9					
2.3 Procedure for Simulation of VIC	14					
3 BENCE MARKING MODELS AND NUMERICAL PARAMETERS	17					
3.1 One-Dimensional Testing Model Stoke's Layer	17					
3.2 Two-Dimensional Testing Model Free Vortex Pair	21					
3.3 Numerical Parameters of Vortex Ring/Moving Wall						
Interactions	25					
4 RESULTS	28					
4.1 Stability Maps	28					
4.2 Vector Plots	28					
5 DISCUSSION	30					
6 CONCLUSIONS	34					
LIST OF REFERENCES						
TABLE						
DTCHDD0						

## LIST OF TABLES

TABLE		
1	The Constant Coefficients of Quasi-Gaussian	
	Redistribution Function	38

# LIST OF FIGURES

Figure		Page
2.1	Sketch of One - Dimensional Vorticity Concentration Profile on Illustrating Diffusion-Induced Velocity	39
2.2	The Geometry and Notation of the Nine-Grid-Point Filter	40
3.1	Sketch Illustrates the Way to Partition Vorticity Field of Boundary Layer. (This is an Example of Three Markers per Unit Length of Wall)	41
3.2	Comparison of Exact and Calculated Velocity Profiles for Stoke's Layer at $\Delta x/\delta=1/6.4$ Which is Used as Initial Condition for The Calculation	42
3.3	Comparison of Exact and Calculated Vorticity Profiles for Stoke's Layer at $\Delta x/\delta=1/6.4$ Which is Used as Initial Condition for The Calculation	43
3.4	The Dependence Between Relative Error and Spatial Resolution for Wall Velocity Calculations (i.e. $u_{calc.}$ at y=0) Using Quasi-Gaussian Filter. Relative Error= $(u_{calc.}/U_w)-1$	44
3.5	Relative Error vs. Temporal Resolution for Diffusion Process Simulation at Wall Layer. Fixed $\Delta x/\delta_e=1/6.4$ for $P=\delta/\delta_e=(68/64)^{1/2}$ , $2^{1/2}$ and $2$	45
3.6	Relative Error vs. Temporal Resolution for Diffusion Process Simulation at Wall Layer. Fixed $\Delta x/\delta_0=1/3.2$ for $P=\delta/\delta_0=(68/64)^{1/2}$ , $2^{1/2}$ and $2$	46
3.7	Relative Error vs. Spatial Resolution for Diffusion Process Simulation at Wall Layer. Fixed $\Delta t/T=0.2875$ for P=8/8 <sub>e</sub> =(68/64) <sup>1/2</sup> , 2 <sup>1/2</sup> and 2	47
3.8	Discrete Vortices Arranged to Simulate Line Vortex.  (This is an Example of N=12)	48

3.9	Comparisons of Vorticity Distributions of Vortex Ring for N=1, N=6 per Lobe and Theoretical Approximation of Maxworthy [1977]. The Vorticity is Calculated by	
	ξ=ð∀/ðx−ðu/ðy	49
3.10	Time-Dependent Radius of Gyration Calculated Using	
	N=6 per Lobe for Pure Diffusion and Hydrodynamic  Motion with Diffusion. The Straight Line is the	
	Theoretical Solution Given by Equation (25)	50
	inedratical Solution Given by Equation (25)	30
3.11	•	
	N=60 per Lobe for Pure Diffusion and Hydrodynamic	
	Motion with Diffusion. The Straight Line is the	
	Theoretical Solution Given by Equation (25)	51
3.12	•	
	N-500 per Lobe for Pure Diffusion and Hydrodynamic	
	Motion with Diffusion. The Straight Line is the	
	Theoretical Solution Given by Equation (25)	52
3.13	The Geometrical Arrangement of Vortex Ring/Noving Wall	
	Interactions for Vortex-In-Cell Numerical Simulations	53
4.1	Stability Maps of Computations with/without Diffusion	
	Model for γ=15° Compared with Experimental Result	
	of Liang[1984]. The Error Bars for Calculated	
	Outcomes are ±2.5 seconds	54
4.2	Computer Generated Vorticity Motion Pictures for an	
	Unstable Interaction which the Line Pair Ingests	
	Wall Layer Fluid as it "Crashes" on the Wall	55
4.3	Computer Generated Vorticity Motion Pictures for an	
	Unstable Interaction which the Line Pair Ingests	
	Wall Layer Fluid as it Turns Away from the Wall	56
4.4	Computer Generated Vorticity Motion Pictures for a	
	Stable Interaction which the Line Pair Leaves the	
	Wall without Breaking Up	57
4.5	Computer Generated Vorticity Motion Pictures for a	
	Stable Interaction in the Absence of Diffusion	
	Process. "Photos" Correspond to The Same Time	
	Step Number as Figure 4.6 Which The Initial	
	Conditions Wars Set Identically to This Case	<b>5 9</b>

4.6	Computer Generated Vorticity Motion Pictures for a Stable Interaction in the Presence of Diffusion Process. "Photos" Correspond to The Same Time Step Number as Figure 4.5 Which The Initial				
	Conditions Were Set Identically to This Case	59			
5.1	Comparisons of Stability Maps for $\gamma=15^{\circ}$ .				
	Calculations without Diffusion for 6 Markers				
	per Lobe were Carried Out by Bartholomew	60			

#### NOMENCLATURE

- D. Ring diameter, the distance between two centers of vortex lobes
- f Fraction, 0 < f < 1
- G Circulation
- I,J Number of cells in x,y direction
- I Angular impulse
- Number of vortex markers used in computer calculation
- r Distance from vortex center
- r, The distance, r, of which contains 100f % vorticity
- Re Reynolds number, pU\_D\_/µ
- R<sub>e</sub> Effective radius of vortex lobe, r
- S Square of the radius of gyration
- S. Initial S at time t.
- t Time
- t. Elapsed time to spread out vorticity to distance R.
- t. Delay time or duration of wall movement
- At Discrete time step length in computer calculation
- T Rotational time parameter for wall layer,  $\delta_{\bullet}/U_{\psi}$
- T. Rotational time parameter for vortex lobe,  $(2\pi R_e)^2/G$
- u, v Convection velocity component in x, y direction
- w, w Diffusion-induced velocity component in x,y direction
- U,V Real velocity component in x,y direction  $\longrightarrow U=u+\widetilde{u}$ ,  $V=v+\widetilde{v}$
- **▼** Velocity vector
- U, Ring speed
- U\_ Wall speed
- x Longitudinal direction

# Ax, Ay Cell size in x,y direction

- y Direction normal to x
- ξ Vorticity
- μ Dynamic viscosity
- ρ Fluid density
- δ Wall layer thickness defined by  $u_8/U_w=1/200$  at time t,  $4(\mu t/\rho)^{0.5}$
- 8. Initial wall layer thickness, 8 at time t.
- γ Initial angle of approach
- η Similarity variable, y/(4μt/ρ)\*\*\*
- ∀ Stream function
- Quasi-Gaussian redistribution function

#### CHAPTER 1

#### INTRODUCTION

Nowadays the complexity of many flows of technological interest makes traditional numerical methods such as finite difference/finite element more difficult to treat problems than ever. One of the reasons for this is the constraints set by the computer: the memory and CPU time needed to resolve the flow features is excessive due to the existence of a wide range of length and time scales. This has led to the development of new computational techniques such as discrete vortex methods.

A problem which illustrates this point is the topic of this thesis —— the evolution of a vortex linepair when it comes into proximity to a moving wall. This is a very common phenomenon. A well-known example is the trailing vortices produced by a jumbo aircraft departing from the runway. A number of experiments have been performed by Harvey and Perry [1971], Barker and Crow [1977] and many others to investigate the behavior of vortex pairs in the presence of the ground. A theoretical approximation for the approach of a vortex pair at right angles to a plane surface in the absence of viscous effects was carried out by Saffman [1979]. Although the reason for the observed rebounding was not clarified, Peace and Riley [1983] pointed out that the rebounding of a vortex pair from a plane boundary is essentially a viscous phenomenon. This is a strong argument in favor of incorporating viscous effects into a discrete vortex method when a vortex ring/wall interactions is to be correctly simulated. We will return to this point below.

The motivation for studying vortex rings comes from Falco [1977] who has postulated that the turbulence production mechanism near a wall is related to interactions between vortex-ring-like eddies and the viscous sublayer. A series of experimental investigations were also performed to study this point of view [Falco, 1978-1982].

In the present work, the study of the vortex ring/moving wall interactions will be modeled in two dimensions using a vortex linepair and a numerical algorithm based upon a discrete vortex method. The simulation will incorporate a viscous diffusion model. This effort will also illustrate the capability of the technique and will allow for the detailed exploration of the physics for the flow field.

A review of the discrete vortex method would have to start with the hand calculations made by Rosenhead [1931] to study a two-dimensional vortex sheet. In the calculations, he was able to use only a few vortices. However, this was the first attempt to simulate a flow by a discrete vortex method. With the evolution of digital computers over the decades, further refinement of vortex techniques have made possible computations which follows hundreds or even thousands of vortices. Accurate time integration schemes have also been used to reduce computational errors.

There are two different ways to evaluate the velocity field induced by the vorticity distribution. One is a grid-free method which is based upon the use of Green's function to compute the velocity by directly summing the velocity field of the individual discrete vortex elements. The other method calculates the stream function defined on an Eulerian grid by solving the Poisson's equation after the vorticity has been spread onto the mesh nodes. The desired velocity is hence obtained by

interpolation: this is termed the Vortex-In-Cell or VIC method. Applications which illustrate the use of the Green's function were carried out by Moore and Saffman [1971]. However, many of these early computations failed to represent the physical phenomena of the flows because point vortices are too singular to yield realistic vorticity distributions. Chorin [1973] first introduced the concept of a finite core to avoid the singularity of a point vortex and hence overcame this problem. Chorin [1978] also used the segments of vortex sheets near boundaries instead of point vortices as the computational elements in studying a piston-cylinder flow. The primary disadvantage of the Green's function formulation is that the computational effort increases as the number of point vortices squared.

To overcome this disadvantage, the VIC technique was developed by Christiansen [1973; which he called "Cloud-In-Cell"] and was applied to the investigation of the motion for a continuous hydrodynamic fluid. This grid-dependent method was also implemented by Baker [1979], Meng and Thomson [1978] and many others in simulating flows. An excellent review of these methods and their applications was done by Leonard [1980] who also provided additional comments contrasting the ability of the two approaches to satisfy conservation principles.

Since both vortex models have the ability to numerically investigate various flows, the selection of suitable technique is understood to be extremely important to avoid any inefficiency and/or inaccuracy. The advantages and disadvantages of each method should be carefully considered when discrete vortex methods are about to be used. Take for example the Green's function scheme which is better suited for high Reynolds number (turbulent) internal flows where the total number

of vortices can be maintained at a small number. The Vortex-In-Cell technique is preferred to treat a problem if a very large number of vortex elements are used (such as external flows).

As mentioned earlier, viscosity plays a key role in the rebounding mechanism for the ring/wall interactions. The viscous effects must be accounted for in the present calculations, of course. Two steps are required to simulate the viscous effects in the computations since the vorticity diffusion term appears in vorticity transport equation. The two steps are as follows. For all time steps,

- 1. Simulate the vorticity dispersion in the flow field.
- 2. Simulate vorticity generation at the boundary to maintain the no-slip condition at the wall.

The former can be included into either the Green's function or VIC method by adding a random walk component or a diffusion induced velocity to the convection velocity of individual vortex element. Chorin [1973] first published the random-walk approach for discrete vortex calculations to reproduce the molecular diffusion process in a stochastic sense. A test of this idea had been performed by Milinazzo and Saffman [1977], who found that the number of vortex elements must be large compared with the Reynolds number if the diffusion caused by viscosity is to be imitated correctly. (There had been some questions raised by Milinazzo and Saffman concerning the rate of convergence: they speculated the rate to be such that the number of vortex blobs N was proportional to the Reynolds number. Roberts [1985] has shown that in actually, careful initialization of the initial distribution reduces this estimate to N<sup>-1/2</sup>Re<sup>-1/2</sup>.) For the sake of simplicity, Kiya et al. [1982] had every discrete vortex endowed with a pre-chosen constant

transverse velocity without regarding to its location when the separation bubble over a two-dimensional blunt flat plate was simulated. This approximation yields a bodily displacement of the shear layer towards the transverse direction. We believe that this model might not be necessarily a bad approximation to reproduce the viscous effect in some special types of flow, but obviously this will not be well-suited in general. Ashurst [1977] used an alternative scheme to approximate the vorticity diffusion by adding a small, but growing, length to the interaction distance r (core size) at each time step. time-dependent core size represented the decay of the strength due to viscous "spreading" of each individual point vortex, which he referred to as "aging". The results of the aging calculations for two-dimensional mixing layer are in good agreement with experimental However, the scheme is restricted since it can not data. incorporated into the VIC technique. This is because the Vortex-In-Cell technique uses a spreading function to redistribute the vorticity from the Lagrangian markers to the grid for the Poisson solver. This redistribution function can be interpreted as an "effective size" of the vortex marker, and is set to a pre-determined constant multiple of the grid length. It has also been shown that "aging" does not necessarily converge for long time simulation [Greengard, 1985].

A deterministic diffusion model designed for the VIC computations is introduced in the present study. The algorithm for this model is based upon using a combination of a modified vorticity gradient approximation with a nine-grid-point, conservative redistribution filter to simulate the viscous spreading of vorticity in the flow field. The computations has been done on a microcomputer in the Turbulence

Structure Laboratory of the Department of Mechanical Engineering at Michigan State University. The solution technique for solving the Poisson's equation was chosen according to the capacity of the microcomputer. In Chapter two the algorithms of inviscid and viscous models are formulated. In Chapter three, two preliminary test cases are examined to check the accuracy and reliability of the diffusion model. The calculated results of vortex linepair/moving wall interactions are compared with the experimental results of Liang [1984] in Chapter four through the use of stability maps and vector plots. A discussion of the no-slip boundary condition will also be included in Chapter five.

#### CHAPTER 2

#### THE THEORY

In the present analysis, a Vortex-In-Cell technique is used to model the ring-wall interactions. The main reason for choosing a VIC method is a matter of economy. The cost of computer time and memory required to update the information for N point vortices would become prohibitive if a Green's function approach were used. This is because the computational work increases as N2 for the Green's function approach, but linearly for VIC. There are approximately 1,300 vortex markers needed to numerically simulate the growing boundary layer of the moving belt for the problem to be studied here. By adapting the VIC model, we may ensure the computation of the motion of such a large number of vortices will be at reasonable cost. In this thesis we will concerned primarily with ideal fluids which are purely two-dimensional and incompressible (uniform density). The principle of the VIC scheme is similar to that of the "Cloud-In-Cell" method: the details are explained in this chapter.

#### 2.1 Governing Formulation for Inviscid Fluids

The Vortex-In-Cell approach implemented here is a mixed Eulerian-Lagrangian description of fluid flow in which the governing formulation of motion is obtained from the vector curl of the Navier-Stokes equation. For a two-dimensional incompressible fluid the vorticity transport equation becomes

$$D\xi/Dt = (\mu/\rho)\Delta\xi , \qquad (1)$$

where D/Dt denotes a total derivative,  $\xi$  is the vorticity,  $\mu$  is the dynamic viscosity,  $\rho$  is the fluid density and  $\Lambda$  is the Laplace operation. Note that in two dimensions the term representing the stretching and rotation of vorticity, which is a three-dimensional process, is identically zero. Consider first the flow of an inviscid fluid (i.e.  $\mu=0$ ). Equation (1) reduces to Euler's equation

$$D\xi/Dt = 0. (2)$$

Before equation (2) is applied, the vorticity must be discretized by partitioning the vorticity into N point vortices. Then

$$\xi = \sum_{i=1}^{N} \xi_i , \qquad (3a)$$

$$G = \sum_{i=1}^{N} G_i , \qquad (3b)$$

where G, the total circulation of vorticity, satisfies the definition :

$$G = \int_{A} \xi \ dA = \int_{C} \overline{\nabla} \cdot d\overline{s} , \qquad (4)$$

where  $\overline{V}$  is the velocity vector and C represents a curve enclosing the area A.

From equation (2), one finds that the vorticity is totally conserved in a two-dimensional flow field from the Lagrangian point of view. This will simplify the updating of vortex markers in the

Lagrangian coordinate by simply moving these markers without changing their strength. Furthermore, one may express the velocity in terms of a stream function  $\Psi$ , which satisfies a Poisson's equation with the vorticity as the source function. If u, v represent the convection velocity components in x, y directions respectively, the formulations take the forms

$$\Delta \Psi = -\xi \quad , \tag{5}$$

$$u = \partial \Psi/\partial y , \qquad (6a)$$

$$\mathbf{v} = -\partial \Psi/\partial \mathbf{x} , \qquad (6b)$$

Note that the boundary conditions of stream function must be initialized before the interior stream function can be solved by equation (5). So far, the approach will approximate the inviscid motion of equation (1). Nevertheless, we must never forget that the general subject of fluid motion encompasses both a viscous diffusion process and bulk fluid motion. The latter ,which results from an inviscid convection process, was described by equations (2), (5) and (6). The former, the viscous part of motion, will be explored and modeled in next section.

#### 2.2 Viscous Diffusion Model

Rather than using the stochastic random-walk approach [Chorin, 1973], a deterministic approximation will be introduced to model the molecular diffusion process. The idea of the diffusion model comes from Fick's first law of diffusion, which states that the mass diffusion rate

of a component is proportional to the concentration gradients. The law can be formulated in the form

$$F_{x} = -D\partial C/\partial x , \qquad (7a)$$

where F denotes the mass flux per unit area, D is the diffusivity and C is the mass concentration of the component. A similar expression could also be written for the diffusion in y direction. Two other laws which are analogous to equation (7a) are the viscous-shear equation and the Fourier law of heat conduction. i.e.

$$\tau = \mu \partial u / \partial y , \qquad (7b)$$

$$q_{x} = -k\partial T/\partial x . (7c)$$

Notice that the physics of equations (7) are also similar. Equation (7b) represents the transport of momentum across fluid layers caused by the velocity gradient, equation (7c) describes the transport of heat by temperature gradients and equation (7a) governs the mass transport by mass concentration gradients.

The three laws illustrated above, especially Fick's first law, give us a heuristic idea that the vorticity transport must occur as a result of diffusion when a vorticity gradient is present. We will now modify and adapt this idea to a diffusion model suitable for vortex calculations. Consider a simple one-dimensional vorticity distribution shown in Figure 2.1. The concentration of vorticity is greater on the right side of this curve than on the left side. A higher concentration

can be interpreted as more discretized vortex markers (in unit strength) per unit length. Thus more markers will move from right to left across the imaginary plane (shown by the dashed line in Figure 2.1) because of molecular processes acting upon the unbalanced concentration. This results in a net vorticity transport from the region of high concentration to the region of low concentration. In short, the hypothesis of the vorticity diffusion illustrates that the rate of vorticity dispersion from a region of concentrated vorticity to an outer non-vortical region is proportional to the local concentration/vorticity gradient.

For the case of pure diffusion, a "diffusion-induced velocity" for a point vortex might be formulated as

$$\tilde{\mathbf{u}} = -(\mu/\rho \xi_{\mathbf{e}}) (\partial \xi/\partial \mathbf{x}) , \qquad (8a)$$

$$\tilde{\mathbf{v}} = -(\mu/\rho\xi_{\bullet})(\partial\xi/\partial\mathbf{y})$$
 (8b)

The coefficient of proportionality between the vorticity gradient and the fictitious diffusion velocity is now dependent on a measure of the local vorticity  $\xi_0$ . In the flows of interest in this discussion, the only possibility that the local vorticity can be zero is if there are no vortex markers present. However, in the calculations, there is no need to sample the vorticity field at that location if there are no vortex markers present. Thus, it may appear there is a singularity in this formulation, operationally, this is not the case. (The singularity, which will blow up the approximation, may appear physically in the central line, where the vorticity gradient is not zero and the

		,
		,

vorticity itself is zero, of some anti-symmetrical vorticity structure. Nevertheless, this can be technically eliminated from the computations.) Accordingly, the local vorticity  $\xi_0$ , which is by no means a zero value in the calculations, will be replaced by the notation  $\xi$  for our studies here.

By using the diffusion theory of vorticity it is easy to numerically predict the dispersion rates of point vortices by simply evaluating the vorticity gradients on each mesh node. Equations (8) hence will approximate the viscous part of the equations of motion (1). The method of fractional steps then states that the total velocity moving the markers is the sum of the convected velocity, which is described by equations (6), and the fictitious diffusion-induced velocity, which is governed by equations (8). Thus

$$U = u + \widetilde{u} \,, \tag{9a}$$

$$V = v + \widetilde{v} , \qquad (9b)$$

where the U, V denote the "real" velocity components, in x, y directions respectively, of a vortex marker. Now the approximation will satisfy the solution of equation (1) at all times in the interior of the computational domain.

It is interesting to note that these results could have been derived using the Navier-Stokes equation. From the conservation of mass for the incompressible two-dimensional flow, we have

$$\partial \mathbf{u}/\partial \mathbf{x} + \partial \mathbf{v}/\partial \mathbf{y} = 0$$
 or  $\nabla \cdot \overline{\mathbf{v}} = 0$ , (10)

where  $\nabla$  denotes the gradient operator. The vorticity transport equation may be written in an alternative form as

$$\partial \xi/\partial t + \nabla \cdot (\xi \overline{V}) = (\mu/\rho) \Delta \xi . \tag{11}$$

if the continuity, equation (10), has been added to equation (1). Similarly the Euler's equation may be written in the form:

$$\partial \xi/\partial t + \nabla \cdot \xi(\overline{V}) = 0 . \tag{12}$$

After rearranging the appropriate terms in equation (11), we obtain

$$\partial \xi/\partial t + \nabla \cdot \left[ \xi \left[ \overline{V} - (\mu/\rho \xi) \nabla \xi \right] \right] = 0 . \tag{13}$$

This result proves, by being compared with equation (12), that the viscous diffusion terms can be interpreted as a contribution to the velocity components of the vortex markers in x and y directions, which we called "diffusion-induced velocities" and is defined in equations (8).

In order to displace these discrete point vortices at each time step, a Predictor-Corrector approximation is used which is a second-order accurate time integration scheme. The algorithm for the Predictor-Corrector is of the form

$$x(t+\Delta t) = x(t) + 0.5\Delta t \Big[ U(t) + U(t+\Delta t) \Big], \qquad (14a)$$

$$y(t+\Delta t) = y(t) + 0.5\Delta t \left[V(t)+V(t+\Delta t)\right], \qquad (14b)$$

where  $\Delta t$  is a unit time step length.

A nine-grid-point filter which was proposed by Bartholomew, my major Professor, is also introduced in the calculations as the spreading mechanism. This improved technique distributes vorticity to the nine nearest neighbor mesh nodes rather than using area weighting to the surrounding four (as used by Christiansen [1973]). This effort will minimize the aliasing conditions that normally appear on the mesh cells [Baker, 1979]. Figure 2.2 provides the geometry and notation of the Quasi-Gaussian redistribution scheme, which is given by

$$\phi(\alpha,\beta) = (A\alpha^{8} + B\alpha^{6} + C\alpha^{4} + D\alpha^{2} + E) \cdot (A\beta^{8} + B\beta^{6} + C\beta^{4} + D\beta^{2} + E)$$

$$for \ 0 \le |\alpha|, |\beta| \le 1.5 , \qquad (15)$$

$$\phi(\alpha,\beta) = 0 \quad otherwise ,$$

where the constants A,B,...B are tabulated in Table 1, and  $\alpha$ ,  $\beta$  are the non-dimensional distances from vortex marker to the grid points. The maximum error occurs at  $\alpha=\beta=0.4$  and is on the order of  $10^{-6}$  with double precision. This scheme conserves the total vorticity both locally and globally, and hence satisfies an important feature of conservation principles. Note that the interpolated velocities also use the same nine-weighting factors. The testing of viscous diffusion model used in conjunction with this redistribution scheme will be illustrated in Chapter three.

#### 2.3 Procedure for Simulation of VIC

The algorithms governing the simulation have been formulated in previous sections. Equation (5) will be easily solved by using a

Compact Non-iterative Poisson Solver [Buneman, 1969]. Although the technique takes more CPU time, we chose it as the Poisson Solver due to the limitation of memory capacity of the microcomputer. In this section the procedure for the VIC calculations will be described as follows. The calculations will follow the thirteen steps in order:

- 1. Determine the computational domain and grid size.
- Determine boundary conditions --- initiate stream function on boundary nodes of the computational domain.
- 3. Partition vorticity field decide on the strength of vortex markers and discretize the continuous vorticity field into point vortices.
- 4. Spread vorticity --- redistribute the marker's vorticity onto its nearest nine mesh points by using equation (15).
- 5. Evaluate viscous effects calculate and normalize vorticity gradients  $(1/\xi)(\partial\xi/\partial x)$ ,  $(1/\xi)(\partial\xi/\partial y)$  on grid points by using a centered difference scheme. Then evaluate equations (8).
- 6. Solve Poisson's equation --- use Buneman's Poisson Solver to evaluate the stream function distribution on interior grid points.
- 7. Evaluate inviscid motion --- obtain the velocity field at grid points by solving equations (6) using centered difference.
- 8. Obtain the "real" velocity field --- sum up the diffusion-induced velocity and inviscid convection motion on each node as defined by equations (9).
- 9. Calculate the velocities of vortex markers --- interpolate velocities back to vortex markers also using the same weighting filter.

- 10. Displace vortex markers --- use equations (14), the Predictor-Corrector integration scheme, as the time marching algorithm to move point vortices.
- 11. Bounce vortices back into flow field (if necessary) --- if a vortex marker crosses the wall at the end of a time step, it will be bounced back into the fluid; i.e. this marker will be returned from  $(x_i,-y_i)$  to  $(x_i,y_i)$ , where the wall is assumed to be at y=0.
- 12. If desired, one can generate new vorticity (if necessary) --create new vortex markers near the wall to maintain the no-slip
  boundary condition if the tangential velocity does not vanish
  at the solid wall. This particular step was not implemented in
  the discussion which follows.
- 13. Repeat steps 4 through 12 for each time step.

  The procedure shown above may be repeated as long as needed.

  Statistical information such as Reynolds stress, fluctuation quantities,

  ... can be obtained by putting numerical probes in the computational flow field.

#### CHAPTER 3

#### BENCH MARKING MODELS AND NUMERICAL PARAMETERS

In the chapter we will present two preliminary test cases in order to obtain a quantitative evaluation of the effects of the approximations made in equations (8). Both testing models employed here are simple and have known analytically solutions. Stoke's layer, the first problem, describing the transport of shear layer caused by viscosity towards the transverse direction, which is an one-dimensional diffusion process. The second testing model is a two-dimensional free vortex pair. growth rate of radius of gyration of the vortex pair provides the information of viscous diffusion rate in two dimensions. To numerically investigate the viscous effects of these testing flows, the viscous diffusion model is incorporated into the Vortex-In-Cell calculations. The accuracy and reliability of the algorithm of the diffusion model will be evaluated by comparing the results of test runs with the theoretical expressions. The target application, the simulations of two-dimensional vortex ring/moving wall interactions, which are governed by some numerical parameters will also be illustrated in the end of this chapter.

### 3.1 One-Dimensional Testing Model -- Stoke's Layer

Now we consider an initially stationary fluid which is bounded by a moving flat wall with a constant speed  $U_{\mathbf{w}}$ . This is a very common flow phenomenon that has a time-dependent boundary layer which is formed on the wall by the effect of fluid viscosity. The governing formulation of

Ķ 12 !1 ٧Ì (i U motion is described by Stoke's exact solution of the Navier-Stokes equation, which takes the form

$$u_{\text{wall layer}} = U_{\text{w}} \left[ 1 - \text{erf}(\eta) \right], \qquad (16)$$

where erf( $\eta$ ) denotes the error function of a similarity variable  $\eta=y/(4\mu t/\rho)^{\theta-\delta}$ .

By means of equation (16) and the definition of vorticity, we will be able to numerically simulate the Stoke's layer. Assume the wall is at y=0 and impulsively started to move with a constant speed at t=0. A (W x H) cm<sup>2</sup> computational domain is chosen and defined by (I x J) grids, where W is the width of the rectangular domain in x-coordinate, H is the height in y direction and I, J are integers such that  $I=W/\Delta x$ ,  $J=H/\Delta y$ . Note that, for simplicity, we always use squares to refine the domain (i.e.  $\Delta x=\Delta y$ ).

Now we may determine the total circulation in the Stoke's layer per unit length  $\Delta x$  of the wall. It is given by

$$G_{\text{total}} = \int_{\text{wall}}^{\text{interior}} \overline{V} \cdot d\overline{s} = \overline{U}_{w} \Delta x$$
 (17)

It is clear that one has to place a number of vortex elements, say N, near the wall per unit length such that each of the elements has strength UAX/N. The way to distribute these discrete vortices is also based upon the definition of circulation. A schematic representation for the example of N=3 for this concept is shown in Figure 3.1 and the transverse locations of these vortices can be presented in equation form

rie:

**5=4** (

Leye

020

loca

obta

the requ

vith

laye

Thez

appl this

init

inte

eçu

reli

[=4]

$$y_m(t,N) = 0.5\delta erf^{-1}[1 - (2m-1)/2N], m = 1,...N$$
 (18)

where the inverse error function  $\operatorname{erf}^{-1}[\operatorname{erf}(\eta)]=\eta$  and  $\delta$  is the boundary layer thickness at time t, which is defined by  $u_\delta/U_\psi=1/200$ ; i.e.  $\delta=4(\mu t/\rho)^{\bullet+\delta}$ . Note that each grid box in the wall layer has at least one marker per cell, and that the number of markers at a given spatial location is proportional to the local vorticity; i.e, the markers overlap. The vorticity field of the computational domain can be obtained after the N-I vortex markers have been distributed.

In order to solve the Poisson's equation (5) by Buneman's solver, the initial conditions of stream function on the boundaries are also required. This can be gained by integrating the exact solution (16) with respect to y. Hence the exact stream function field of Stoke's layer at time t may be stated as

$$\Psi_{\text{wall layer}} = \int u_{\text{wall layer}} dy$$

$$= U_{\text{w}} \left[ y \cdot \text{erfc}(\eta) + 2(\mu t/\pi \rho)^{0.5} (1 - \exp^{-\eta^2}) \right], \quad (19)$$

where  $\operatorname{erfc}(\eta)=1-\operatorname{erf}(\eta)$  is the complimentary error function. We will apply Abramowitz and Stegun's rational approximation [1964] to evaluate this function. The error is on the order of  $10^{-7}$ . Now we may initialize the calculations by using the vorticity distribution in the interior and the exact boundary condition of stream function from equation (19).

Before further investigation, we are going to evaluate the reliability of the approach illustrated above. Let  $\Delta x=\Delta y=0.5$ cm, I=4J=128, N=10,  $U_w=10$ cm/sec,  $\mu/\rho=10^{-2}$ cm<sup>2</sup>/sec, t=64sec (i.e.  $\Delta x/\delta=1/6.4$ )

and the numerical probes placed at x=16cm.

Figure 3.2 shows the comparison of exact and calculated velocity profiles. Figure 3.3 shows the comparison of vorticity profiles at the same condition. Obviously, the outcomes of calculations are in good agreement with the theoretical curves except very near the wall. This is because the redistribution filter smooths sharp peaks such as the peak in the vorticity distribution of the exact solution. There are approximately an -11% error which occurs at y=0 in the calculated velocity profile and -10% error in the vorticity profile. In fact, these relative errors are strongly dependent on the ratio  $\Delta x/\delta$ , which is shown in Figure 3.4. Fortunately, this error could be partially reduced, when the ratio  $\Delta x/\delta$  is appropriately small, by forcing the x-component velocity at each wall node to be  $U_w$ . This correction will be used in all of the wall layer simulations afterwards.

To further investigate the effect of molecular viscosity which is supposed to diffuse, or spread out, concentrations of vorticity near the wall, different lengths of time step have been studied at the same rotational time parameter  $T=\delta_0/U_w=1/23$  where  $\delta_0$  is the wall layer thickness at time  $t_0$ . Simulations are starting from  $t_0$  and ending at t. For each time step length, calculations have been made for three cases:  $\delta/\delta_0=(68/64)^{0.5}$ ,  $2^{0.5}$  and 2.

Figure 3.5 shows the dependence between relative error and temporal resolution at the same spatial resolution  $\Delta x/\delta_0=1/6.4$ . The relative error defined here takes the form

Relative Error = 
$$1/N \sum_{m=1}^{N} \left[ (y_{m_{calc.}}/y_{m_{exac.}}) - 1 \right]$$
, (20)

where  $y_{mexac}$  is evaluated using equation (18). As expected, the error increases as At increases. However, there is no noticeable change when the ratio At/T is smaller than 1. Figure 3.6 also shows the same feature at constant  $\Delta x/\delta_0=1/3.2$ . The optimum time step length hence can be determined according to these two figures and other factors such as the expense of CPU time.

Figure 3.7 shows the relative errors with different spatial resolutions at fixed nondimensional time step length  $\Delta t/T=0.2875$ . The ultimate resolution that could be examined was  $\Delta x/\delta_0=1/12.8$  due to the memory constraint of the microcomputer. It shows that the higher spatial resolution yields the higher accuracy as predicted. In other words, the growing wall layer can be successfully simulated by applying our viscous diffusion model as long as the resolution parameters  $\Delta t/T$  and  $\Delta x/\delta_0$  are chosen moderately small. The calculated results are quite good especially for the case of short time simulation  $\delta/\delta_0=(68/64)^{0.5}$  which corresponds to 4 seconds of real time. This will satisfy the needs of our final application since the interacting time for vortex ring and moving wall is always shorter than 5 seconds of real time.

# 3.2 Two-Dimensional Testing Model --- Free Vortex Pair

The decay of a two-dimensional vortex pair in the absence of a solid wall has also been studied using our viscous diffusion model to investigate the accuracy of the approach. Consider a single line vortex having position  $(x_e, y_e)$  and strength  $G_{pv}$ . In polar coordinates, the velocity component  $v_{\Theta}$  is given as

$$v_{\Theta}(r,t) = (G_{pv}/2\pi r) \left[1 - \exp(-\rho r^2/4\mu t)\right].$$
 (21)

The circle of radius r which contains 99% of the vorticity can be shown, using equation (4), to be

$$r = 2[(\mu t/\rho) \ln[G_{pv}/(G_{pv}-0.99G_{pv})]]^{0.5}.$$
 (22)

Now we use N vortex markers with strength  $G_i$  so that  $G_{pv} = \sum_{i=1}^{N} G_i$  to represent the single line vortex of initial effective radius  $r_i = R_e$ . Thus  $t_e = \rho R_e^2 \left[ 4\mu \cdot \ln[G_{pv}/(G_{pv} - 0.99G_{pv})] \right]^{-1}$  is the elapsed time to spread out vorticity to this effective size. From equation (22), we can infer that the radius  $r_f$  of a circle which possesses some vortex markers with total strength  $fG_{pv}$  can be formulated as

$$r_{f} = 2 \left[ (\mu t_{e}/\rho) \ln [G_{pv}/(G_{pv}-fG_{pv})] \right]^{0.5}$$

$$= R_{e} \left[ -0.21715 \cdot \ln(1-f) \right]^{0.5}, \qquad (23)$$

where f is a fraction. This formulation will be used to distribute vortex markers in the effective circle. Since it was derived from an exact representation (21) of a line vortex, the realistic vorticity field ought to be conserved after being discretized. A schematic diagram illustrating the arrangement for N=12 is shown in Figure 3.8.

Consider the N vortex markers, the i-th marker is placed at  $(x_i,y_i)$ . The square of the radius of gyration S is defined by

$$S = -2I_a/G_{pv} , \qquad (24)$$

where  $I_a = -0.5 \sum_{i=1}^{N} G_i \left[ (x_i - x_e)^2 + (y_i - y_e)^2 \right]$  is the angular impulse with respect to  $(x_e, y_e)$ . In a viscous unbounded fluid, S grows linearly with

time. The exact solution takes the form

$$S = S_a + 4\mu t/\rho , \qquad (25)$$

where  $S_e$  is the initial square of radius of gyration at time  $t_e$ . By means of this exact solution, we will be able to evaluate the outcomes of simulations later on.

The stream function field induced by the single line vortex in an unbounded fluid can be obtained by the formula

$$\psi_{x_{\bullet},y_{\bullet}} = -(G_{pv}/4\pi) \ln \left[ (x-x_{\bullet})^{2} + (y-y_{\bullet})^{2} \right]. \tag{26}$$

The evolutions of a vortex pair which encompasses two line vortices with equal magnitude of strength  $G_{\overline{p}v}$  but opposite sign could be numerically studied by placing N vortex markers at each lobe using equation (23). If  $D_r$ , the distance between the two centers of lobes, and  $U_r$ , the speed of the vortex pair, are known, we may evaluate the strength for each lobe.

$$G_{pv} \text{ (lower)} = (\pm) 2\pi U_r D_r . \tag{27}$$

The initial values of stream function on boundaries can be calculated using equation (26) by superposition

$$\psi_{\text{vortex pair}} = \psi_{x_u, y_u} + \psi_{x_1, y_1}, \qquad (28)$$

where  $(x_u, y_u)$  and  $(x_1, y_1)$  are the centers of upper lobe and lower lobe

respectively.

Figure 3.9 shows the vorticity distributions through upper lobe for vortex rings simulated using N=1 and N=6 at  $D_x$ =3R<sub>e</sub>=5.3 $\Delta x$ . Compared with an exponential distribution typified by sech<sup>2</sup>r [Maxworthy, 1977]. Apparently, better agreement for larger N.

To examine the validation of the viscous diffusion model, two cases, (i) pure diffusion and (ii) hydrodynamics plus diffusion, have been investigated with the same initial condition. We set  $D_r=3R_e$ , I=2J=64,  $\Delta x=\Delta y=0.25$ cm and choose the values of  $D_r$ ,  $U_r$  such that  $\Delta x/R_s=1/4$  and Reynolds number  $Re=\rho U_r D_r/\mu=1000$ .

The initial rotational time for each lobe is  $T_r = (2\pi R_e)^3/G_{pv}$ . It was found that the results did not have any noticeable change when the unit time step lengths  $\Delta t$  were chosen to be less than  $T_r/60$ . Computations have been done with this value of  $\Delta t$  for N=6, N=60 and N=500. The total simulation time is  $3T_r$ .

Figure 3.10 shows the normalized square of the radius of gyration  $S/S_0$  as a function of  $t/T_T$  for both cases (i) and (ii) with N=6. S used here is the average value of upper and lower lobes. The exact solution (25) is also shown for comparison. The relative error is about -25% after three rotations.

Figure 3.11 and Figure 3.12 show the results for N=60 and N=500 respectively. The size of the relative error is about -8% for N=60 and -4% for N=500 at integration time 3T<sub>r</sub> in case(i). Apparently the number of vortex markers N must be large enough, say the order of 10<sup>2</sup> in this problem, to yield the realistic vortex structure and hence reproduce the viscous diffusion. However, the rapid improvement in accuracy from N=6 to N=60 should also be noted. In order to save CPU time and memory

As an example, N=60 is accurate enough to be used instead of N=500 to resolve the vortex structure. It can be concluded that the approximations of vorticity diffusion in two dimensions by using our viscous model are in good agreement with the theoretical results, but the resolution of the vortex structure must be in moderately high order.

## 3.3 Numerical Parameters of Vortex Ring/Moving Wall Interactions

The two-dimensional vortex ring/moving wall interactions are essentially the interactions between line-vortex pairs and a moving wall. Figure 3.13 shows the geometrical arrangement of this flow field for VIC simulations. Some numerical parameters which governs this problem are introduced as follows.

γ : the initial angle of approach.

U\_/U\_: the ratio of ring speed to wall speed.

 $\delta_{\rm e}/{\rm D_r}$ : the ratio of wall layer thickness to ring diameter.

Since the vortex ring/moving wall interactions can have evolutions which are either stable or unstable, the governing parameters illustrated above could be related as the representation

$$(\delta_{\bullet}/D_{\underline{r}})$$
 = Function( $\gamma$ ,  $\overline{U}_{\underline{r}}/\overline{U}_{\underline{w}}$ ). (29)

We define a stable interaction as one in which the vortex ring turns away from the wall without ingesting wall layer fluid. An unstable interaction ingests wall layer fluid before/as the ring turning away

from the wall. These definitions were developed by Liang [1984]. The critical lines which distinguish the stability and instability of evolutions can be acquired by systematically varying these related parameters.

The algorithms for simulating Stoke's wall layer and line-vortex pair by discrete vortices have been fully described in Sections 3.1 and 3.2 respectively. The stream functions on boundaries of computational domain are the only values that have to be determined to initialize the calculations. However, we know that the stream function field induced by a line vortex in the presence of solid wall can be obtained by modifying equation (26) to give

$$\psi^{(w)}_{x_{\bullet},y_{\bullet}} = \psi_{x_{\bullet},y_{\bullet}} - \psi_{x_{\bullet},-y_{\bullet}}. \tag{30}$$

Consequently, the stream function of this problem can be obtained from equations (19) and (30) by superposition. Then

$$\psi_{\text{ring/moving wall}} = \psi^{(w)}_{x_u,y_u} + \psi^{(w)}_{x_1,y_1} + \psi_{\text{wall layer}}$$
 (31)

This approach for the boundary conditions has been discussed in detail by Baker [1979].

The computations have been done for  $\gamma=15^{\circ}$  with one marker per lobe for the line-wortex pair and 10 markers per unit length of wall for Stoke's layer. We set I=4J=128,  $\Delta x=\Delta y=0.5$ cm,  $\Delta t=1/80$ sec,  $U_r=64.4$ cm/sec,  $D_r=2.65$ cm and the initial height of linepair is at y=6.23cm. Two parameters,  $\delta_{\circ}/D_r$  and  $U_r/U_w$ , range from 0.9 to 2 and 0.4 to 0.8 respectively.

Simulations with/without viscous diffusion model have been carried out at the same initial conditions. No new vorticity has been generated during calculations. This means that the no-slip condition at wall might not to be satisfied all the time. The importance of viscous diffusion model will be evaluated by comparing the calculated outcomes with experimental results via stability maps and flow visualizations in next chapter.

### CHAPTER 4

#### RESULTS

An LSI 11/23 microcomputer has been charged with all the efforts of computations. The outputs will be presented, quantitatively by means of stability maps and qualitatively via computer generated vector plots, in the following sections.

## 4.1 Stability Maps

Figure 4.1 shows the stability map comparisons for  $\gamma=15^{\circ}$ , which uses delay time t, as the unit of y coordinate. The maps of numerical simulations with/without viscous diffusion model are computed to within  $\pm 2.5$  second error bars. It is found that the calculations are in better agreement for higher delay times than for lower delay times when compared with the experimental stability map.

### 4.2 Vector Plots

Figures 4.2 to 4.6 show the computer generated vector plots of vortex linepair/moving wall interactions with different initial conditions. These plots indicate the evolutions of linepairs when they come closer to the wall. Both the linepairs and wall are moving from left to right. Only those vortex markers which lie inside the graphics display domain (indicated in Figure 3.13) are shown. The vectors represent the instantaneous velocities of vortex markers. The outline around the linepair stands for the concentrated vorticity region of ring lobes, which is for reference only.

Figure 4.2 sequence showing the ingestion of wall layer fluid into the lower lobe as the linepair "crashes" right on the wall. This is the type of strong breakup where the linepair did not turn away from the wall.

Figure 4.3 shows a linepair breakup after ingesting wall layer fluid as it moves away from the wall. This type of breakup is different from that in Figure 4.2.

Figure 4.4 indicates the type of survival of linepair which leaves the wall without breaking up. Note that the numerical simulations from Figure 4.2 to 4.4 were all done with the viscous diffusion model.

Figures 4.5 and 4.6 show the evolutions of liftup of linepairs for calculations were done without the diffusion model and done with diffusion model respectively. All the initial conditions of these two figures were set identically, but the latter included the vorticity diffusion process while the former did not. Apparently we can find, by observation, that the viscosity makes the linepair turn away from the wall earlier and also smooths the concentrated wall vorticity. Discussion of the overall results will be in next chapter.

#### CHAPTER 5

#### DISCUSSION

The results presented in this work demonstrate that it is possible to simulate the experimental vortex ring/moving wall interactions, when the wall layer is thick, by a two-dimensional linepair calculation. Although the detailed comparisons of stability maps are not in good agreement, and as expected the agreement becomes DOOT 28 three-dimensional effects begin to dominate the interaction. In view of the fact that the two-dimensional simulations have shown the ability, by means of vector plots, to reproduce the various flow phenomena of the stable/wastable evolutions of the three-dimensional ring/wall interactions, we can infer that the overall stability/instability of the vortex ring/moving wall interactions is adequately described by two-dimensional mechanisms. This interpretation indicates importance of two-dimensional effects in this flow field. Nevertheless, the stretching of the vortex tube element and other three-dimensional effects are important in determining details of the flow such as the mixing process near the wall, Reynolds stress, fluctuations and etc. which will be significantly effected by stretching/reorientation of the vortex structure.

In the vortex ring/moving wall interactions, the three-dimensional effects become more important when the rings come closer to the wall. This is because the rings, when they near the wall, will be under the influence of vortex stretching which may cause, for example, the amplifying of wall layer fluid ingestion and hence breaking up faster.

For the case of thin wall layer thickness, the ring can easily approach the wall so that the subsequent evolution of the ring is dominated by the effects of three-dimensional mechanisms. This is the reason why the two-dimensional calculations failed to yield good results in the thin wall layer thickness region which corresponds to the short delay time region in Figure 4.1.

Since the vortex rings were roughly approximated by the line-vortex pairs in the computations, a question arose —— would the overall outcomes be improved if more vortex markers were employed, instead of one marker per lobe, to represent the structure of ring lobes? Bartholomew clarifies this by using six vortex markers per ring lobe to re-calculate the ring/wall interactions in the absence of viscous diffusion process. The efforts yield a slightly better result in the stability map which is shown in Figure 5.1, but the agreement in the short delay time region is still poor. This result enhances our belief that the three-dimensional effects in the short delay time region are the major effects responsible for the poor comparison of the numerical simulations in this region.

Unfortunately the viscosity seems not very important in the two-dimensional vortex pair/moving wall interactions since there is no difference, within ±2.5 seconds error bars, between the stability maps for calculations done with/without the viscous diffusion model. However, one will find out that the effects of viscosity in the flow field may not be so trivial when the computer generated vector plots in Figures 4.5 and 4.6 are carefully compared. These two figures indicate that the computations with the viscous diffusion model have successfully created two physical phenomena which have never been shown in the

inviscid calculations. One is the vorticity gradients have been smoothed via the diffusion process of wortex markers, which can be easily seen by the growth of boundary layer thickness for instance. The other is the vortex ring, in a stable interaction, turns away from the wall strongly through the influence of viscosity. This feature proves that the viscosity does play a significant role in the rebounding mechanism, as mentioned earlier in Chapter one, of the ring/wall interactions. In other words, we can expect that the critical line in the stability map for computations with the diffusion model will be shown lower in some degree than that in an inviscid calculations if finer numerical investigations are made; i.e. reduce the size of error bars to, for example, ±0.5 seconds and see the differences in the viscous/inviscid stability maps. Nevertheless, a huge time is required to do so under the current facility which needs approximately 26 hours of execution time to run for just one ring/wall interaction. Due to the time limitation, we do not refine the calculations to achieve more precise results.

The no-slip condition is also an important characteristic of viscous effects at the wall surface. Since our viscous diffusion model is only designed for simulating the molecular diffusion process in the flow interior, no particular step was employed to maintain the no-slip boundary condition which might not be satisfied all the time during the calculations. This, of course, introduced some error which may not be negligible in the overall results. To maintain the no-slip condition, new vorticity should be generated if the tangential velocity is found not vanish at the wall during the simulations. In fact, the algorithm described in Section 3.1 had been called to create new point vortices in

the vicinity of the surface to satisfy the no-slip boundary condition. This attempt, however, failed to represent the reality of the boundary layer since too many weak vortices had been generated very close to the wall. This gives us a lesson that care must be taken to avoid spurious results if the new vorticity creation process at the solid surface and the subsequent motions of these vortices are about to be correctly modeled. Although we decided not to include this step in the calculations, we believe that the use of finite vortex sheets as the newly created elements could be a better way to model the creation process at the wall, but there is no hard evidence on this matter and the question is open.

There are also many other error sources such as the truncation error, the accumulated round-off error, ... have not been mentioned. In general, the error contributions by these sources are relatively small and not well understood.

#### CHAPTER 6

#### CONCLUSIONS

Numerical simulations of the vortex ring/moving wall interactions done with some success using the two-dimensional Vortex-In-Cell technique. In these calculations the effect of molecular viscosity diffusion was approximated by adding a deterministic velocity component for each discrete vortex. This "diffusion-induced velocity" was defined in terms of a modified gradient approximation which was obtained from a transformation of the vorticity transport equation. have tested the viscous diffusion model on both one and two-dimensional time-developing flows and achieved satisfactory computer-generated vector plots also show that the use of the diffusion model changed the local details of the rebounding phenomenon in the ring/wall application, but did not appear in the overall stability maps within ±2.5 second error bars. More computer time is needed to resolve this paradox. From the practical point of view, we feel that this model is a simple and effective scheme to represent the vorticity diffusion process in the flow interior.

The qualitative features of the ring/wall interactions are well reproduced by this numerical method, but close quantitative comparisons with experiments indicate that in the real flow the three-dimensional deformation of vortex filaments becomes significant in the thin wall layer zone of stability map, so that the VIC technique in two dimensions can poorly simulate there. In order to further improve the calculated outcomes, the inclusion of three-dimensional flow representations

appears to be required. With this, the viscous diffusion would be more important due to the thinner wall layers encountered by the ring. However, we do not have the means to extend the computations to three dimensions under the current computing capability.

On the LSI 11/23 microcomputer it took 311.5 seconds to advance the positions of 1282 point vortices for each time step. Approximately 40% of this time was taken up by executing Buneman's Double-Cycle-Reduction routine. This compact Poisson solver is not quite efficient in speed, but the big advantage is its memory requirement fits small computers.

Future work will try to include follows in the calculations when the VAX 11/750 computer is available:

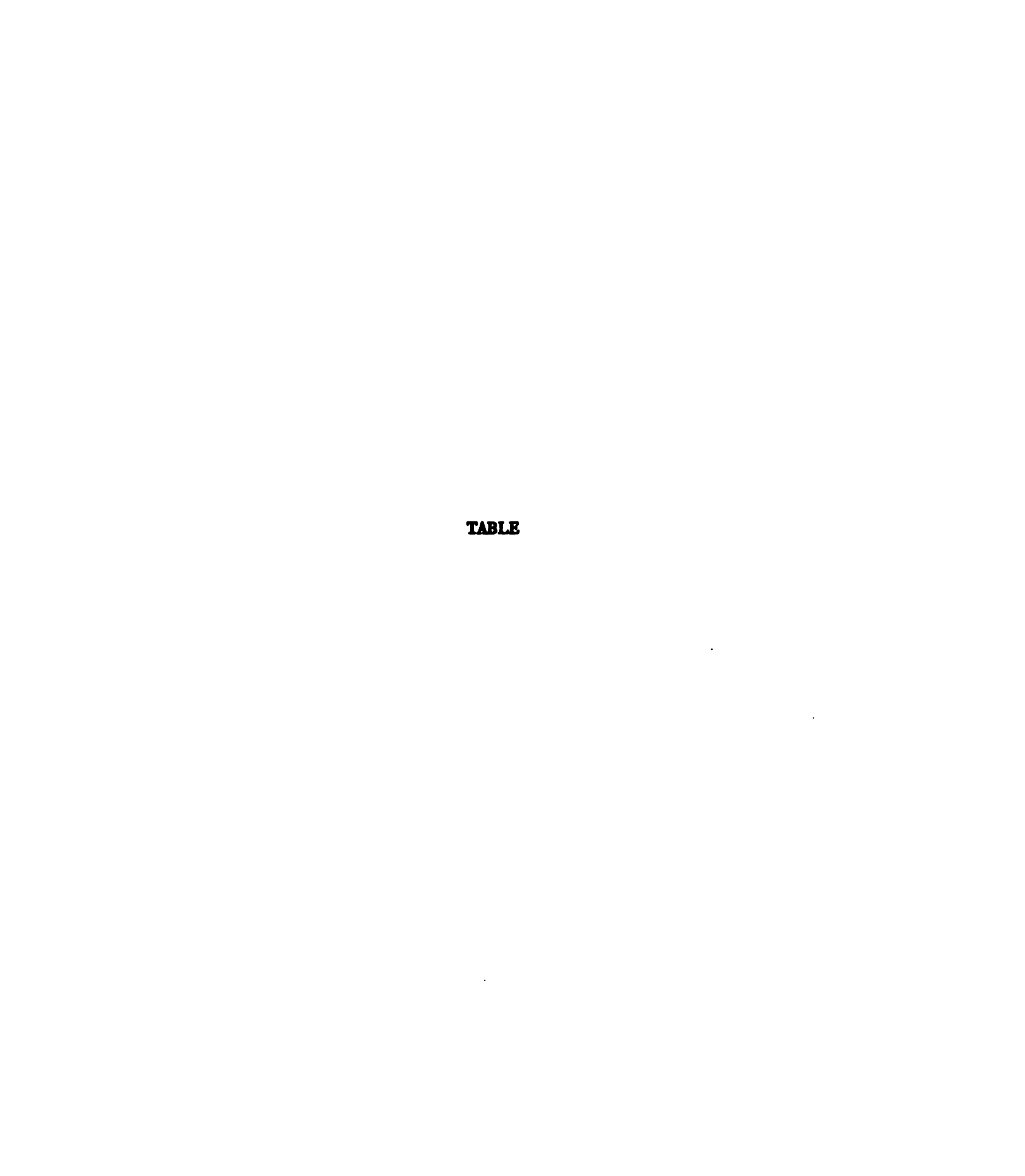
- (1) Flow mechanisms in three dimensions.
- (2) Fast-Fourier-Transform routine as the Poisson solver.
- (3) Suitable model for treating no-slip boundary condition.



### LIST OF REFERENCES

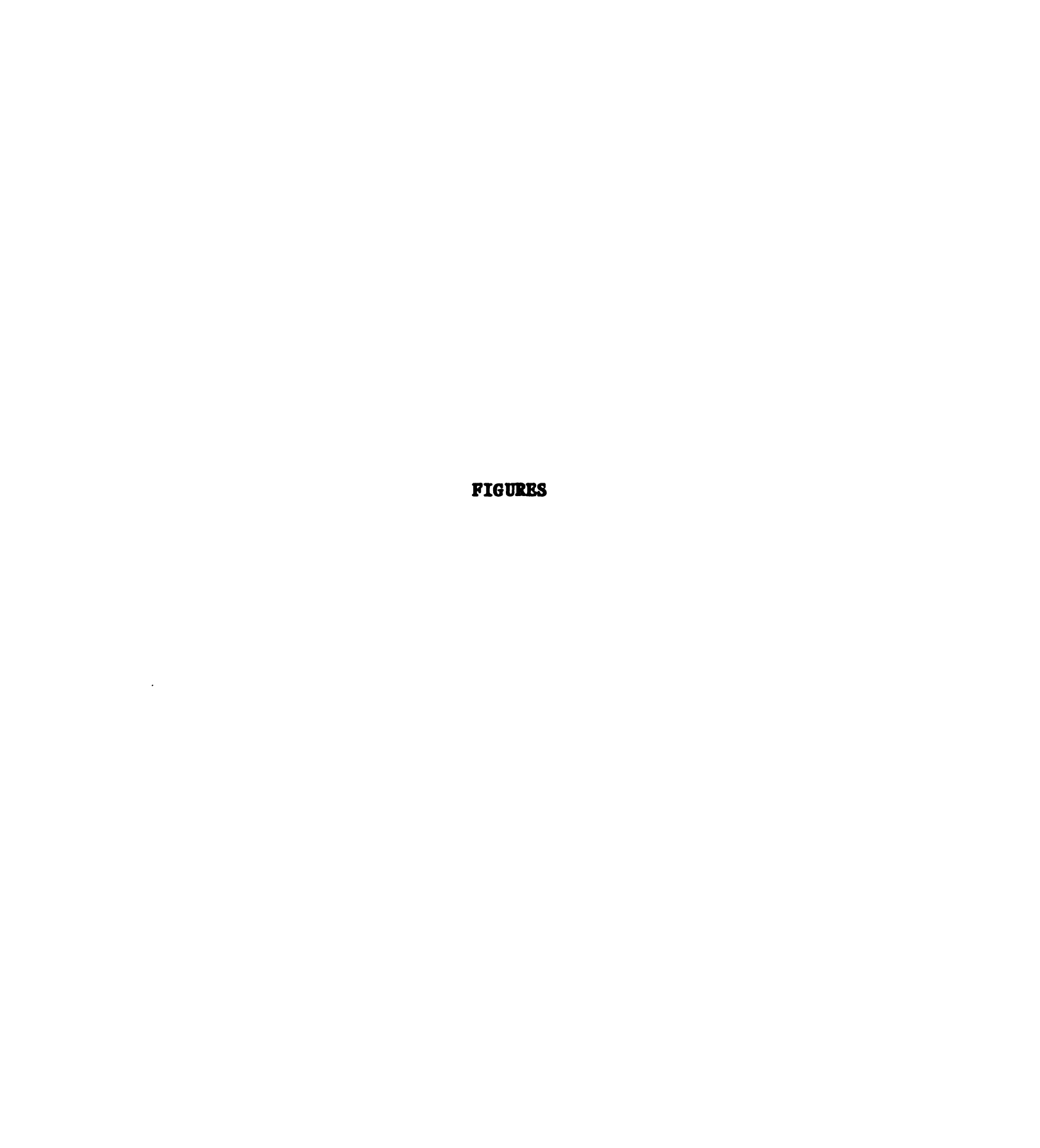
- 1. Abramowitz, M., Stegun, I. A. 1964. Handbook of Mathematical Functions. Page-299
- 2. Ashurst, W. T. 1977. Numerical simulation of turbulent mixing layers via vortex dynamics. Sandia Lab. Rep. SAND77-8612
- 3. Baker, G. R. 1979. The "Cloud in Cell" technique applied to the roll up of vortex sheets. J. Comput. Phys. 31:76-95
- 4. Barker, S. J., Crow, S. C. 1977. The motion of two-dimensional vortex pairs in a ground effect. J. Fluid Nech. 82:659-671
- 5. Buneman, O. 1969. Compact non-iterative Poisson solver. Stanford Univ., Calif. Inst. for Plasma Research. SU-IPR-294 UNCLAS
- 6. Chorin, A. J. 1973. Numerical study of slightly viscous flow. J. Fluid Nech. 57:785-796
- 7. Chorin, A. J. 1978. Vortex sheet approximation of boundary layers. J. Comput. Phys. 27:428-442
- 8. Christiansen, J. P. 1973. Numerical simulation of hydrodynamics by the method of point vortices. J. Comput. Phys. 13:363-379
- 9. Falco, R. B. 1977. Coherent motions in the outer region of turbulent boundary layers. Phys. of Fluids 20:124-132
- 10. Falco, R. E. 1978. The role of outer flow coherent motions in the production of turbulence near a wall. AFOSR/Leigh
- 11. Falco, R. E. 1982. A synthesis and model of turbulence structure in the wall region. ICHMT/IUTAM Conference on the Structure of Turbulence in Heat and Mass Transfer
- 12. Greengard, C. 1985. NOTE The core spreading vortex method approximates the wrong equation. J. Comput. Phys. 61:345-348
- 13. Harvey, J. K., Perry, F. J. 1971. Flowfield produced by trailing

- vortices in the vicinity of the ground. AIAA J. 9:1659-1660
- 14. Kiya, M., Sasaki, K., Arie, M. 1982. Discrete-vortex simulation of a turbulent separation bubble. J. Fluid Nech. 120:219-244
- 15. Leonard, A. 1980. Vortex methods for flow simulations. J. Comput. Phys. 37:289-335
- 16. Liang, S. Y. 1984. Vortex ring/Moving wall interactions. Thesis, Mechanical Engr. Dept. of Mich. St. Univ.
- 17. Maxworthy, T. 1977. Some experimental studies of vortex rings. J. Fluid Mech. 81:465-495
- 18. Milinazzo, F., Saffman, P. G. 1977. The calculation of large Reynolds number two-dimensional flow using discrete vortices with random walk. J. Comput. Phys. 23:380-392
- 19. Moore, D. W., Saffman, P. G. 1971. Structure of a line vortex in an imposed strain. Aircraft Wake Turbulence, ed. Olsen, J. H., Goldburg, A., Rogers, M. 339-354
- 20. Peace, A. J., Riley, N. 1983. A viscous vortex pair in ground effect. J. Fluid Nech. 129:409-426
- 21. Roberts, S. 1985. Accuracy of the random vortex method for a problem with non-smooth initial conditions. J. Comput. Phys. 58:29-43
- 22. Rosenhead, L. 1931. The formation of vortices from a surface of discontinuity. Proc. R. Soc. London Ser. A 134:170-192
- 23. Saffman, P. G. 1979. The approach of a vortex pair to a plane surface in inviscid fluid. J. Fluid Mech. 92:497-503
- 24. Thomson, J. C. S., Meng, J. A. L. 1978. Numerical studies of some nonlinear hydrodynamic problems by discrete vortex element methods. J. Fluid Nech. 84:433-453



Coefficient	Value Tabulated in Double Precision
A	1.7636684303351 X D-3
В	-3.3950617283950 X D-2
С	2.5738536155203 X D-1
D	-7.2296626984130 X D-1
Е	6.6517857142857 X D-1

Table 1 The Constant Coefficients of Quasi-Gaussian Redistribution Function



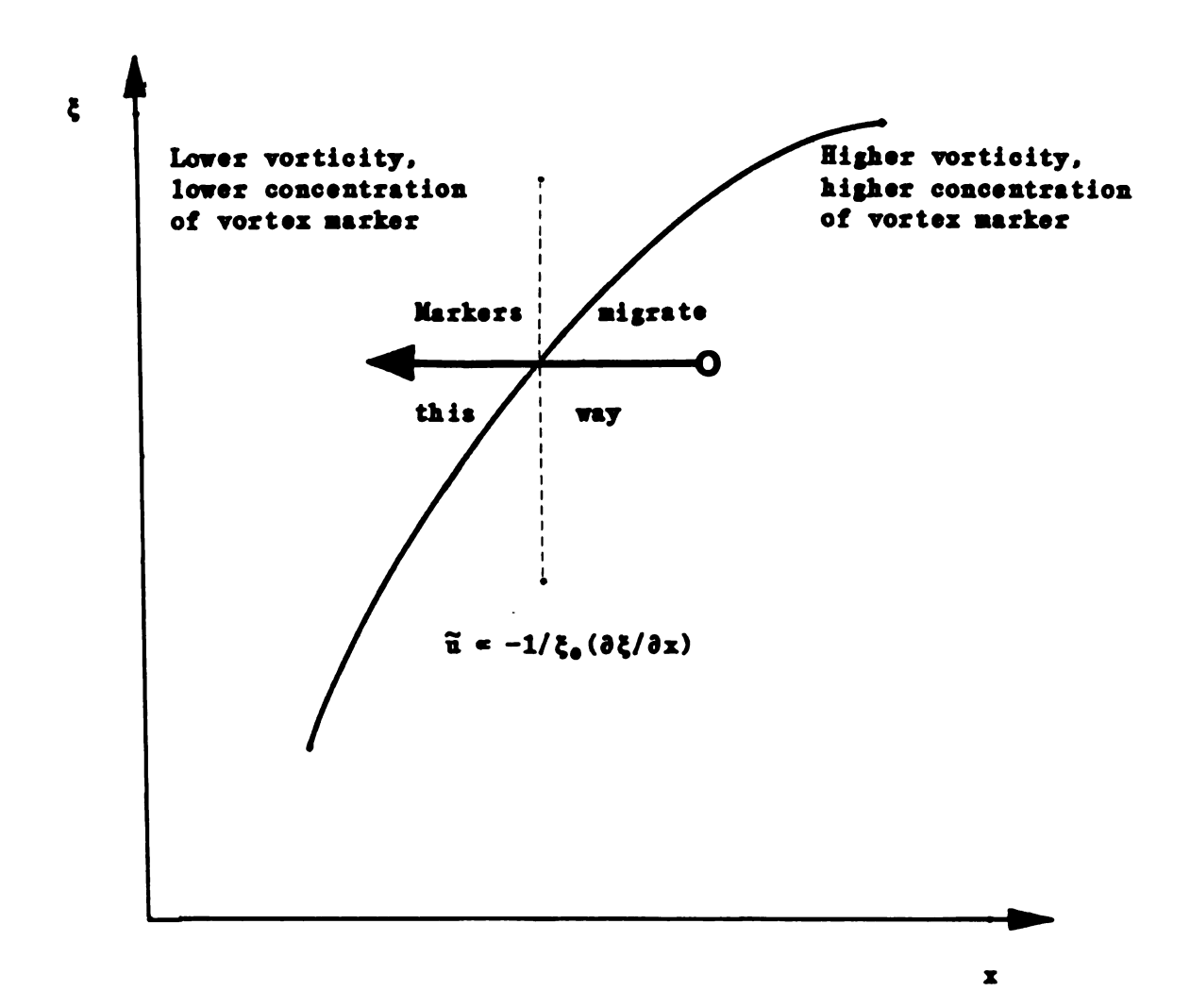
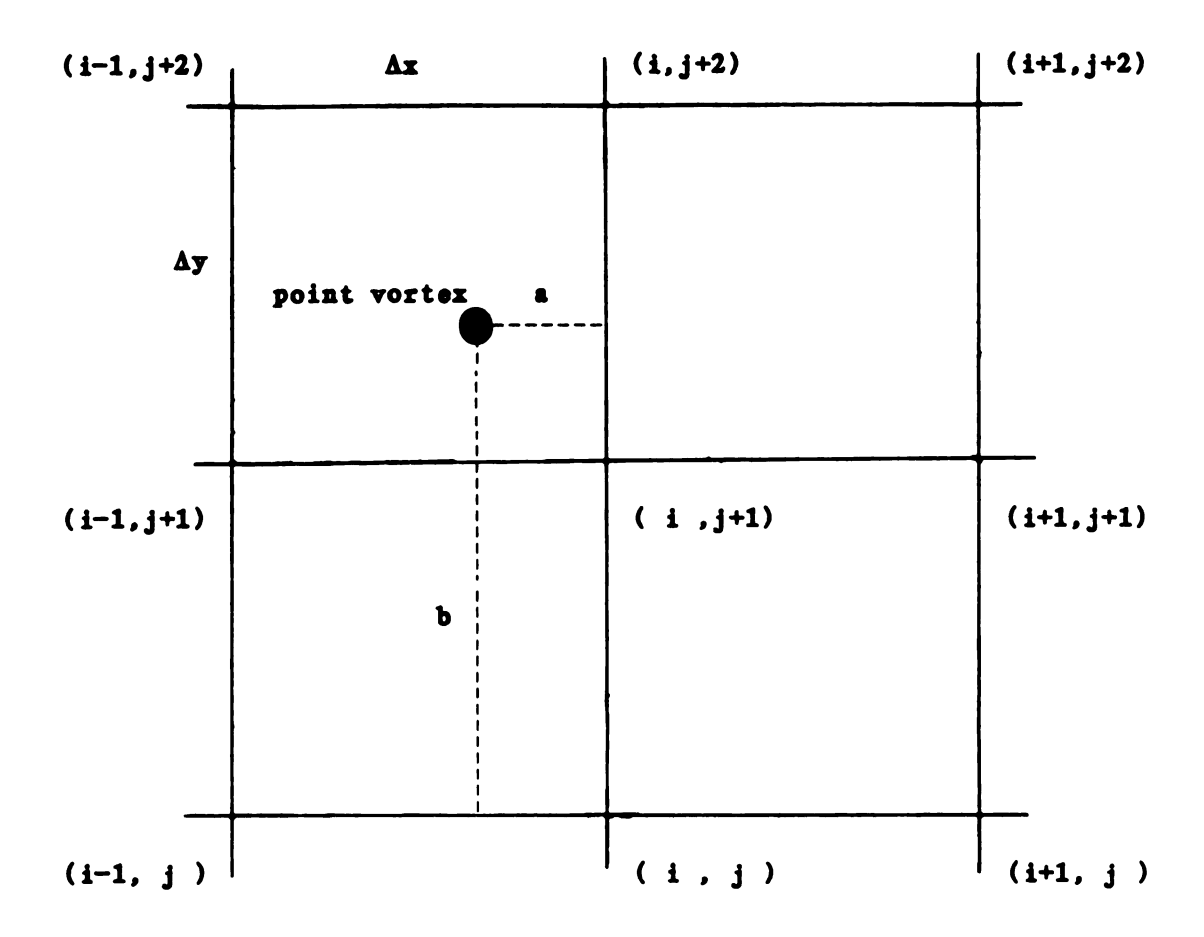


Figure 2.1 Sketch of One - Dimensional Vorticity Concentration Profile on Illustrating Diffusion-Induced Velocity



For node ( i , j ):  $\alpha = a/\Delta x$  $\beta = b/\Delta y$ 

Figure 2.2 The Geometry and Notation of the Nine-Grid-Point Filter

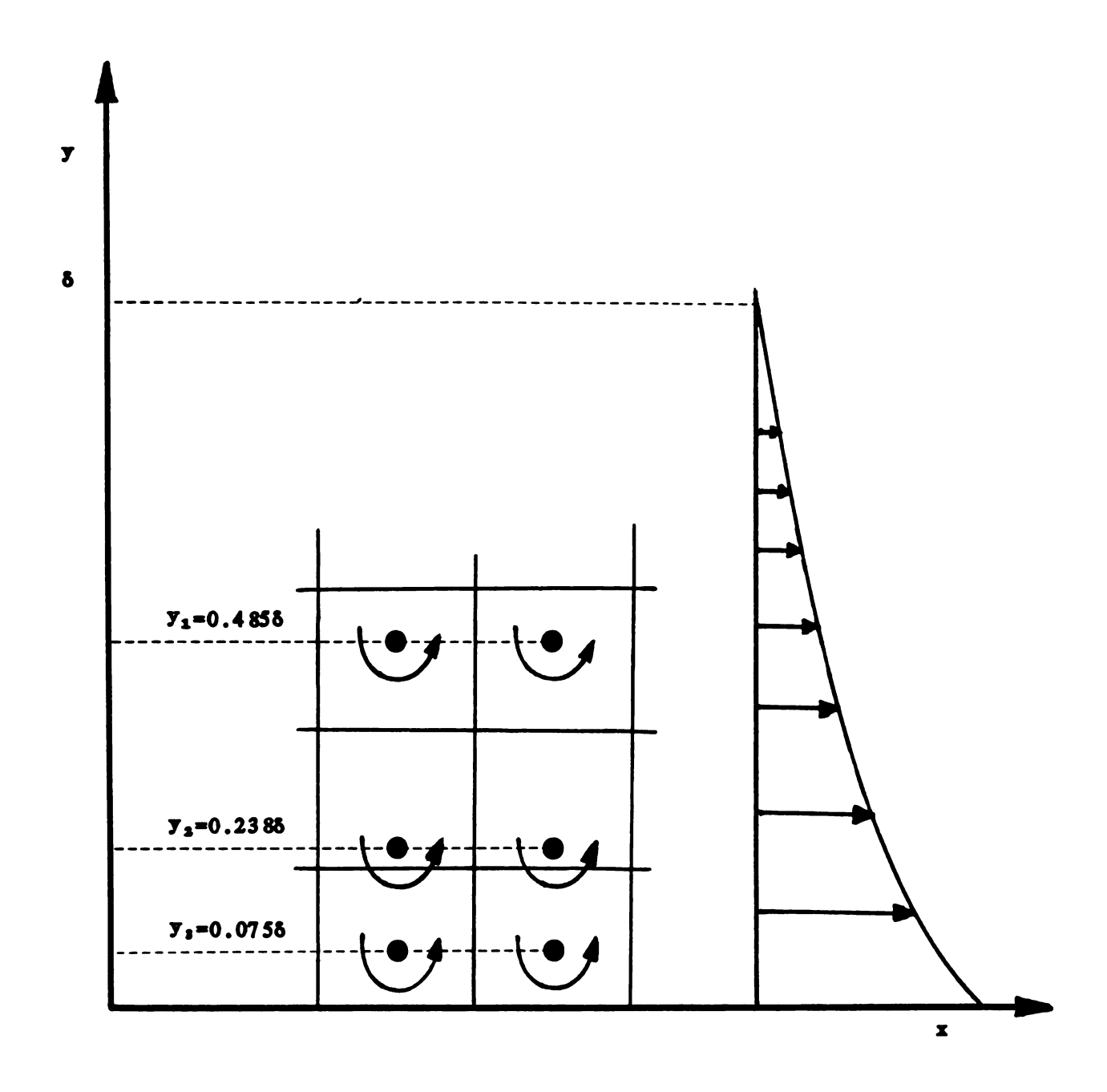


Figure 3.1 Sketch Illustrates the Way to Partition Vorticity Field of Boundary Layer. (This is an Example of Three Markers per Unit Length of Wall)



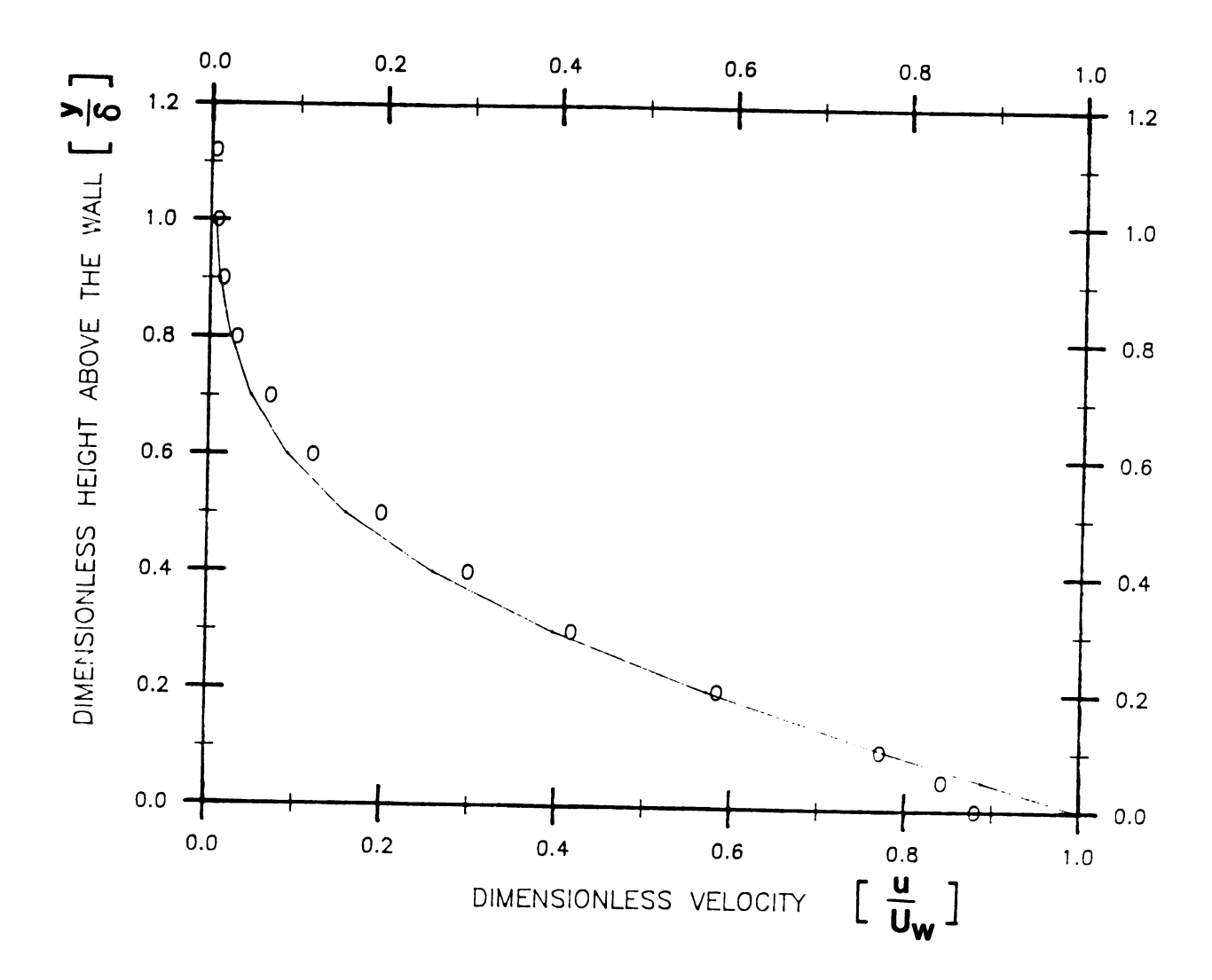


Figure 3.2 Comparison of Exact and Calculated Velocity Profiles for Stoke's Layer at  $\Delta x/\delta = 1/6.4$  Which is Used as Initial Condition for The Calculation

0 : CALCULATED -- : STOKES SOLUTION

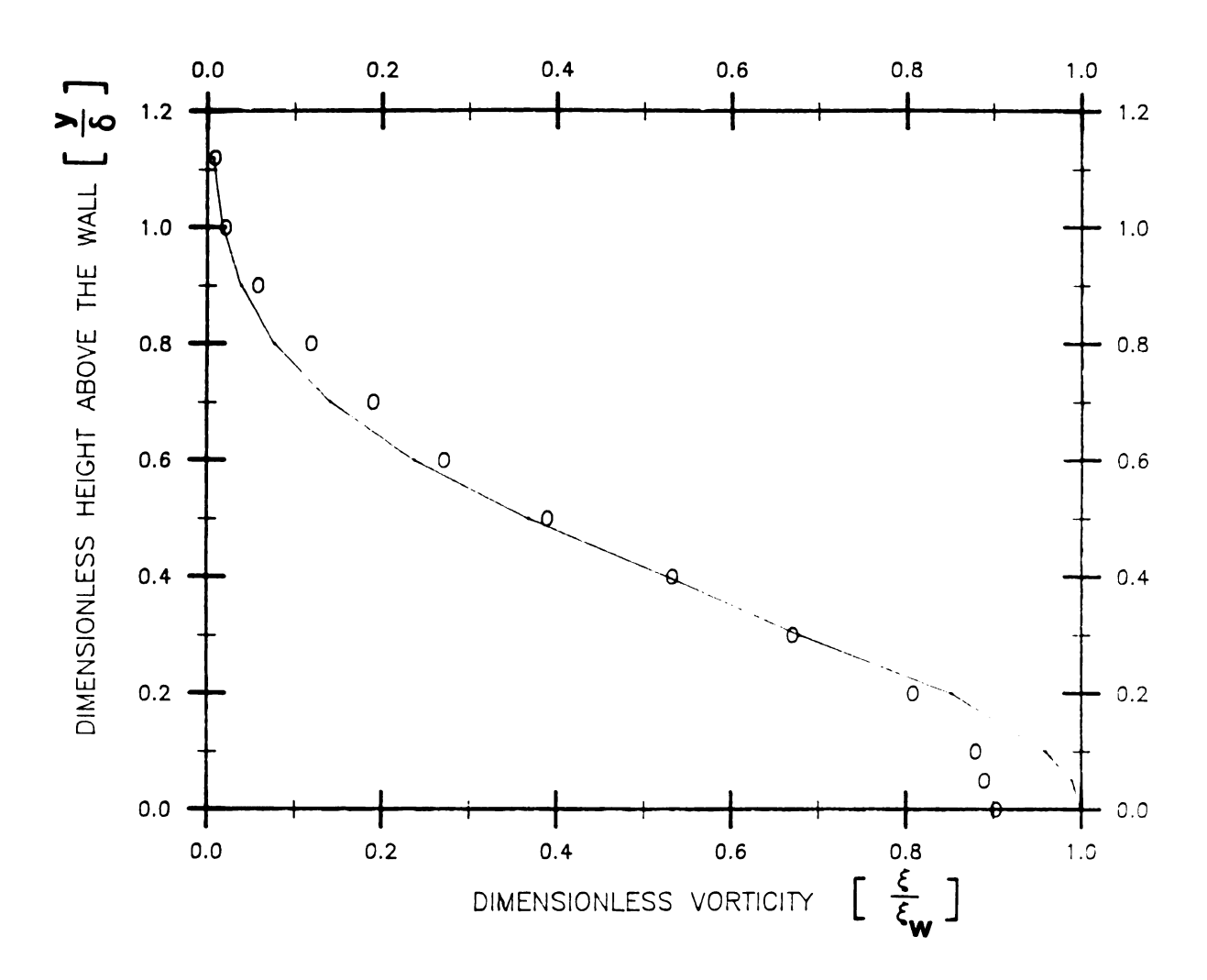


Figure 3.3 Comparison of Exact and Calculated Vorticity Profiles for Stoke's Layer at  $\Delta x/\delta = 1/6.4$  Which is Used as Initial Condition for The Calculation

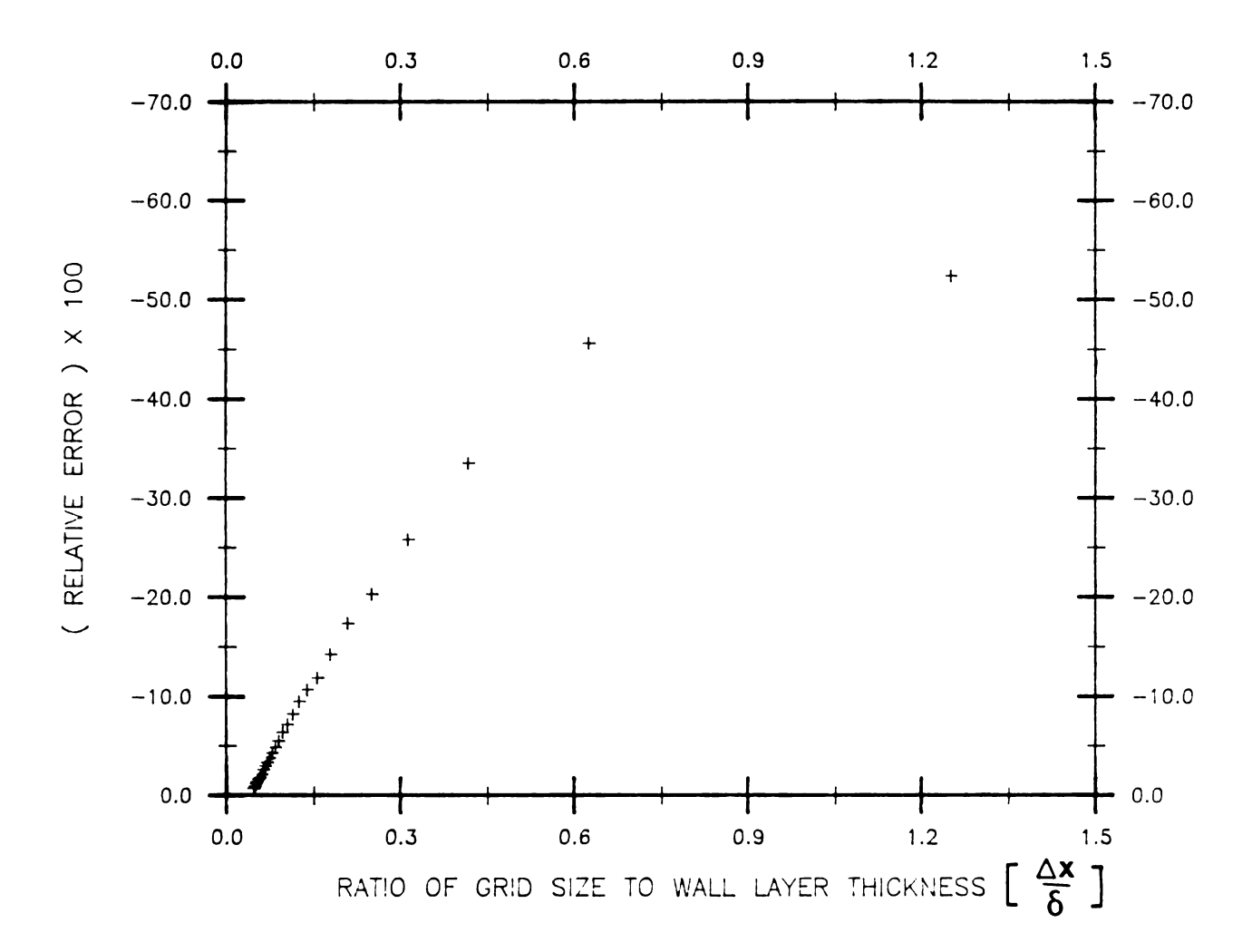
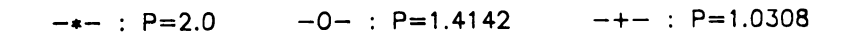


Figure 3.4 The Dependence Between Relative Error and Spatial Resolution for Wall Velocity Calculations (i.e.  $u_{calc.}$  at y=0) Using Quasi-Gaussian Filter. Relative Error= $(u_{calc.}/U_w)-1$ 



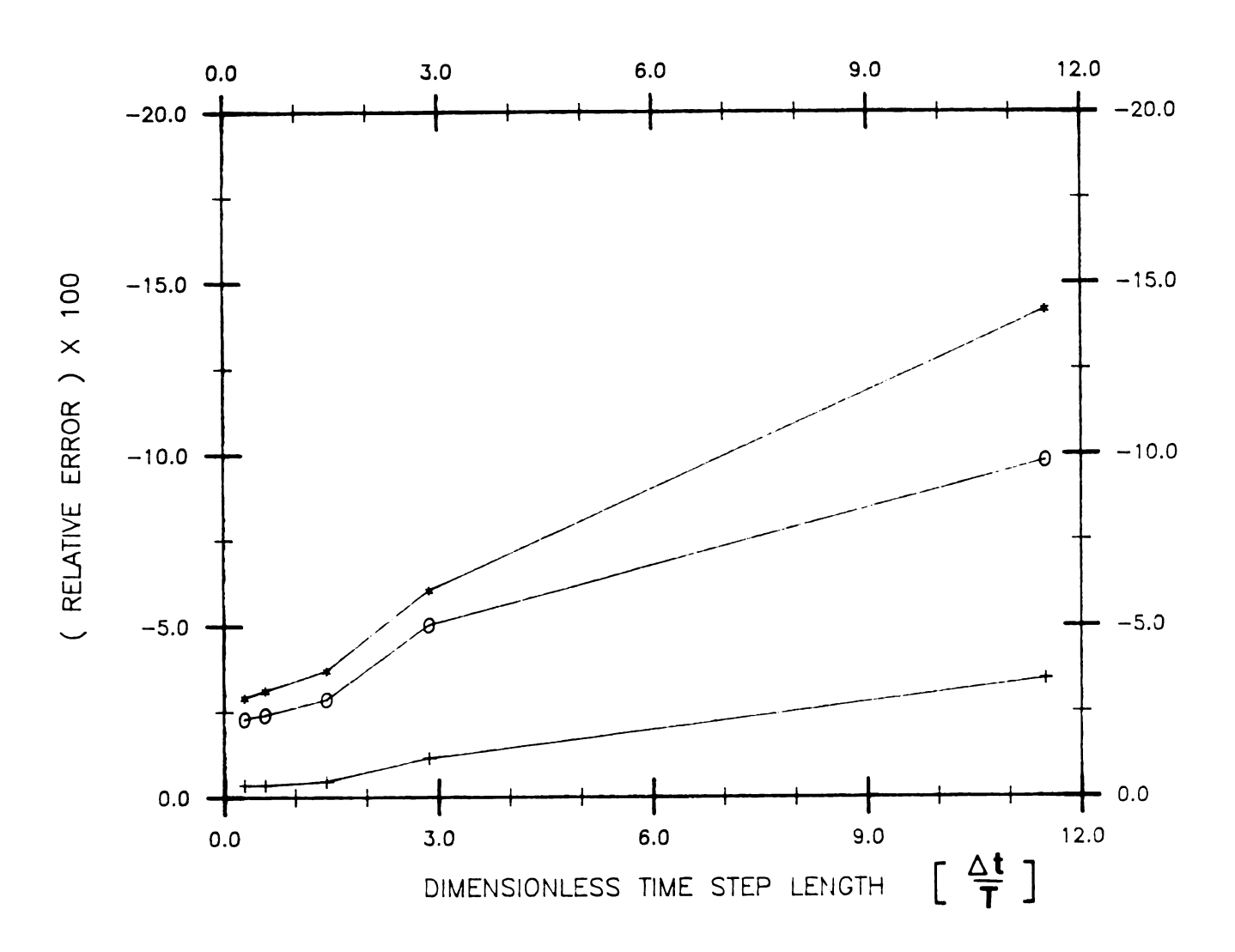


Figure 3.5 Relative Error vs. Temporal Resolution for Diffusion Process Simulation at Wall Layer. Fixed  $\Delta x/\delta_0=1/6.4$  for  $P=\delta/\delta_0=(68/64)^{1/2}$ ,  $2^{1/2}$  and 2

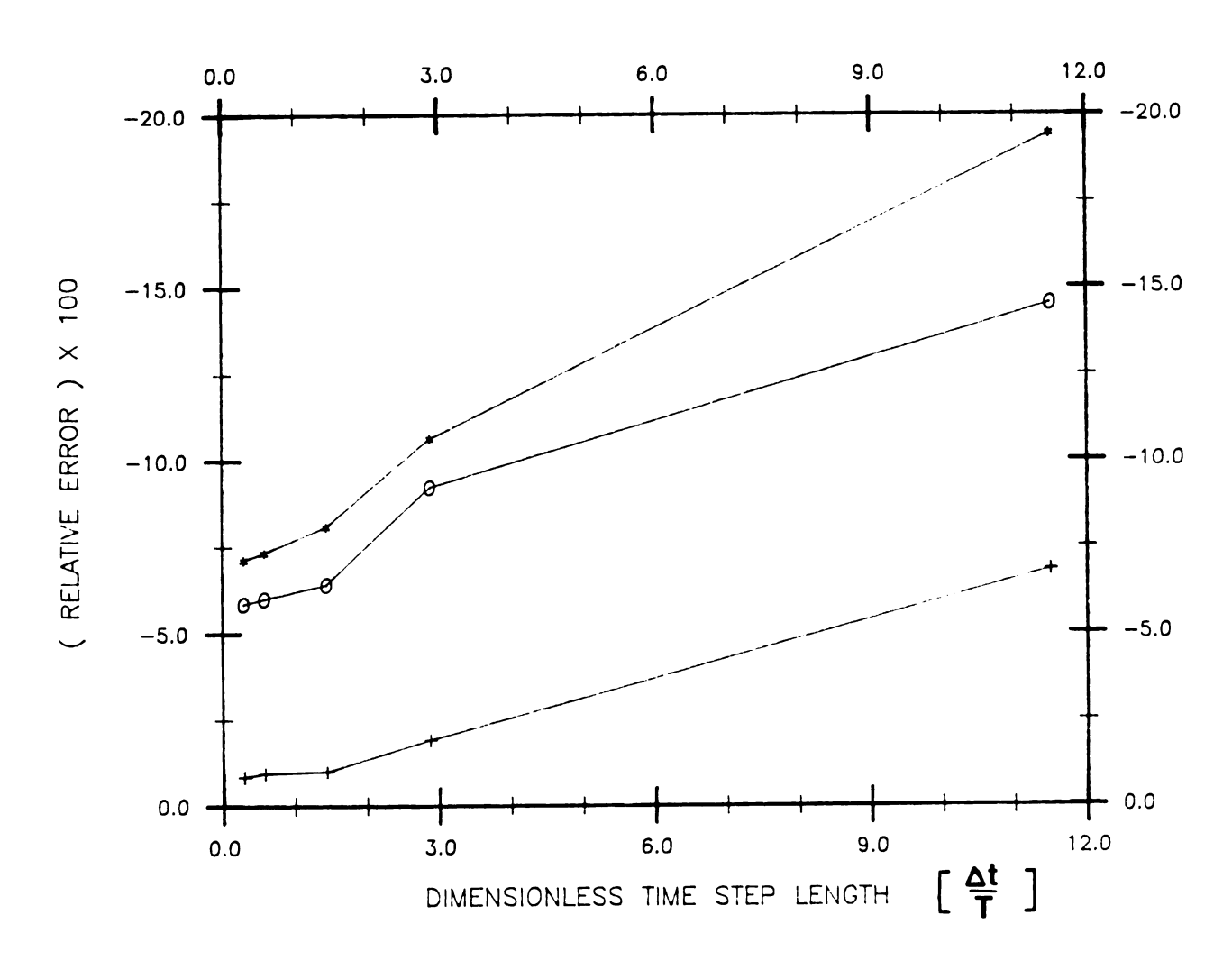


Figure 3.6 Relative Error vs. Temporal Resolution for Diffusion Process Simulation at Wall Layer. Fixed  $\Delta x/\delta_0=1/3.2$  for P= $\delta/\delta_0=(68/64)^{1/2}$ ,  $2^{1/2}$  and 2

-+- : P=2.0 -0- : P=1.4142 -+- : P=1.0308

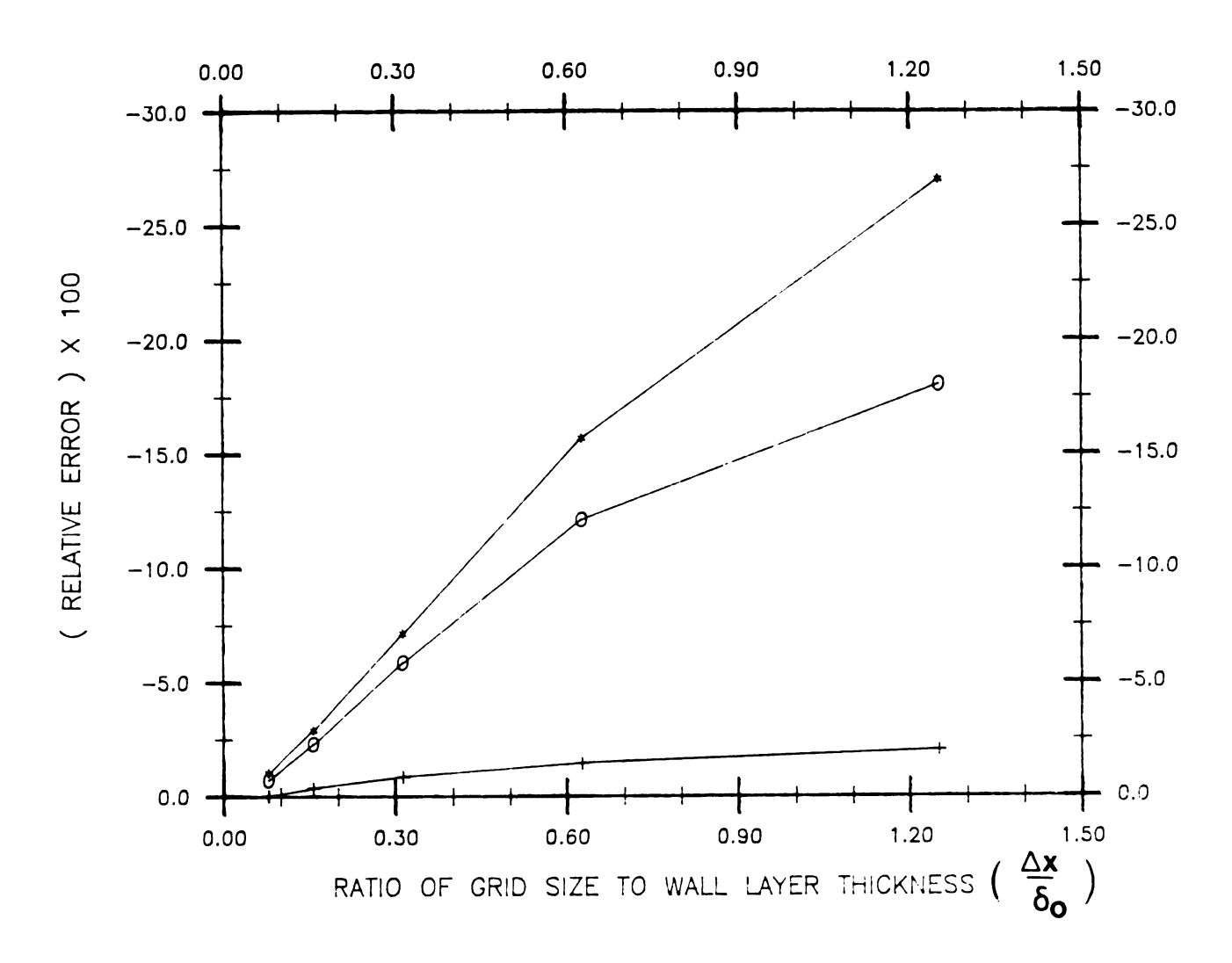


Figure 3.7 Relative Error vs. Spatial Resolution for Diffusion Process Simulation at Wall Layer. Fixed  $\Delta t/T=0.2875$  for  $P=\delta/\delta_0=(68/64)^{1/2}$ ,  $2^{1/2}$  and 2

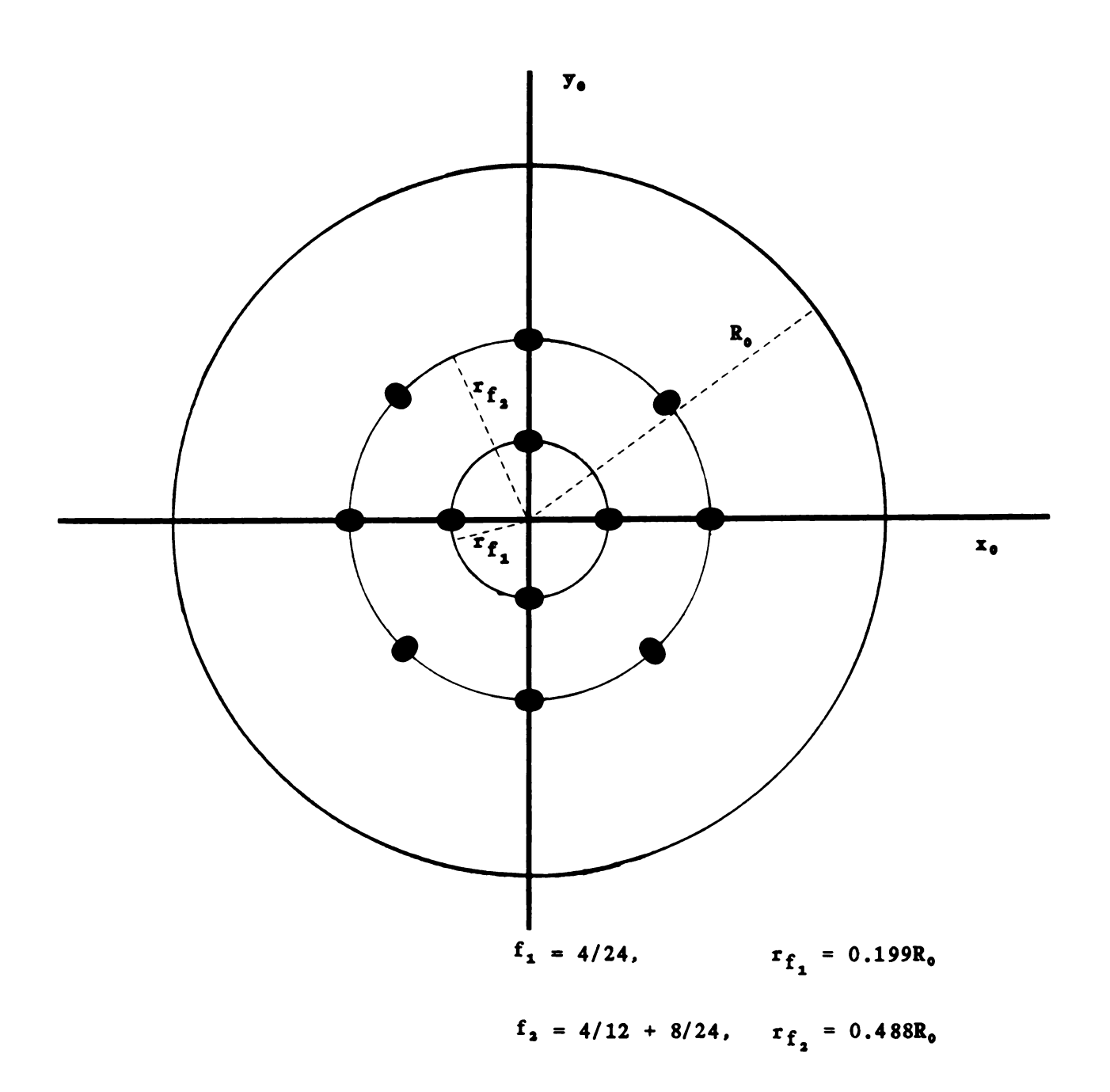
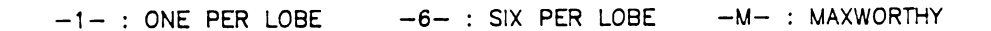


Figure 3.8 Discrete Vortices Arranged to Simulate Line Vortex. (This is an Example of N=12)



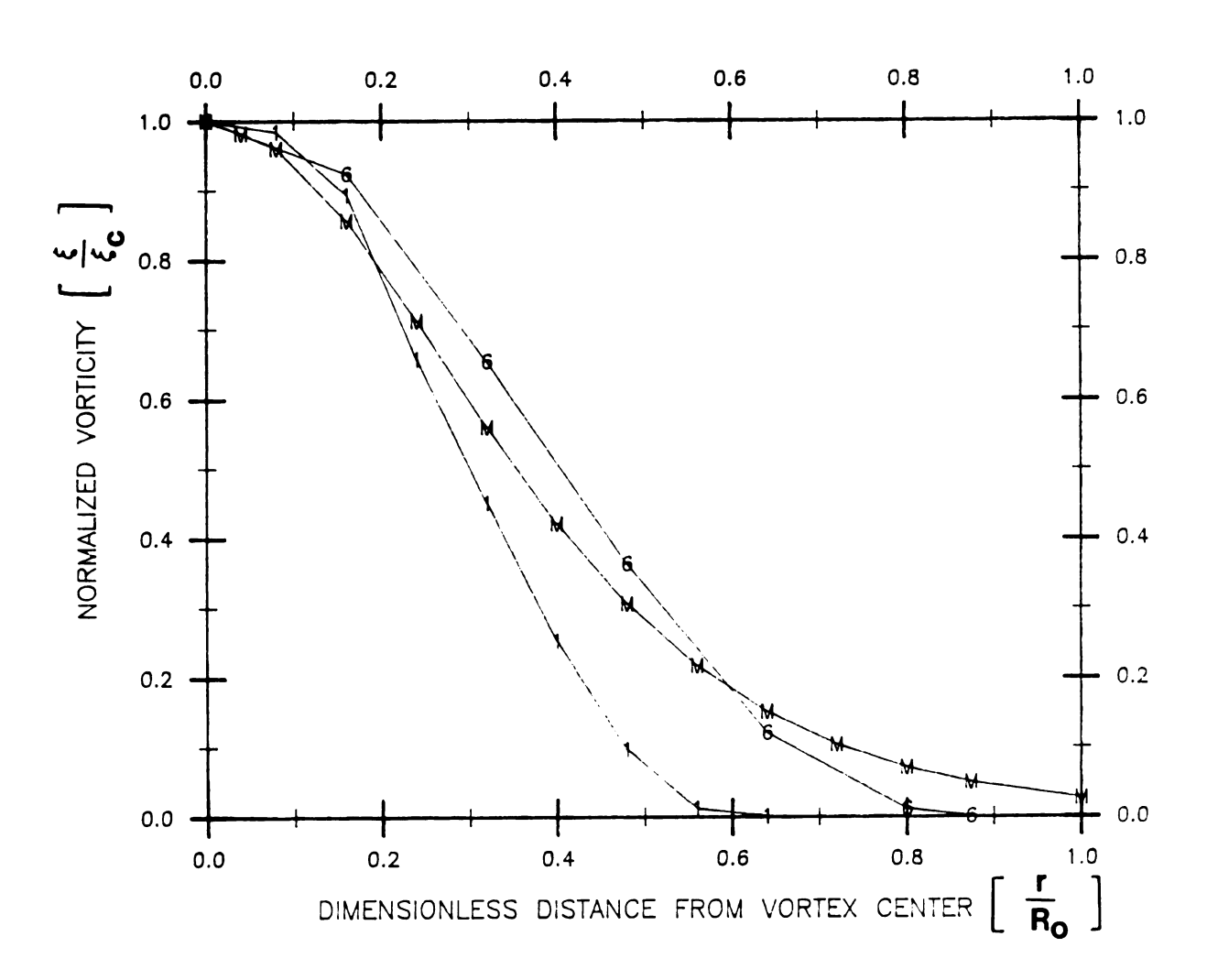


Figure 3.9 Comparisons of Vorticity Distributions of Vortex Ring for N=1, N=6 per Lobe and Theoretical Approximation of Maxworthy [1977]. The Vorticity is Calculated by  $\xi=\partial v/\partial x-\partial u/\partial y$ 

-1- : ONE PER LOBE -6- : SIX PER LOBE -M- : MAXWORTHY

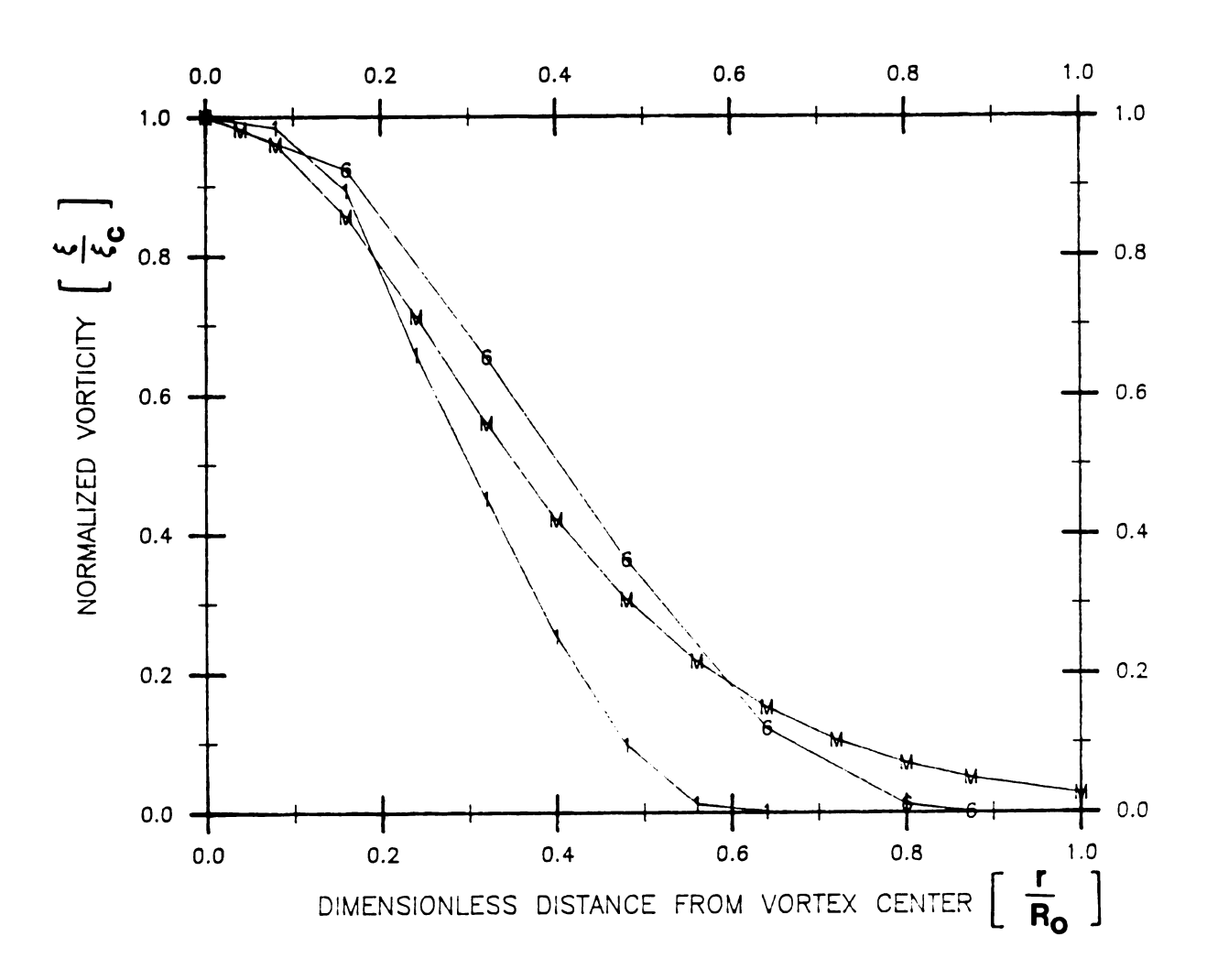


Figure 3.9 Comparisons of Vorticity Distributions of Vortex Ring for N=1, N=6 per Lobe and Theoretical Approximation of Maxworthy [1977]. The Vorticity is Calculated by  $\xi=\partial v/\partial x-\partial u/\partial y$ 

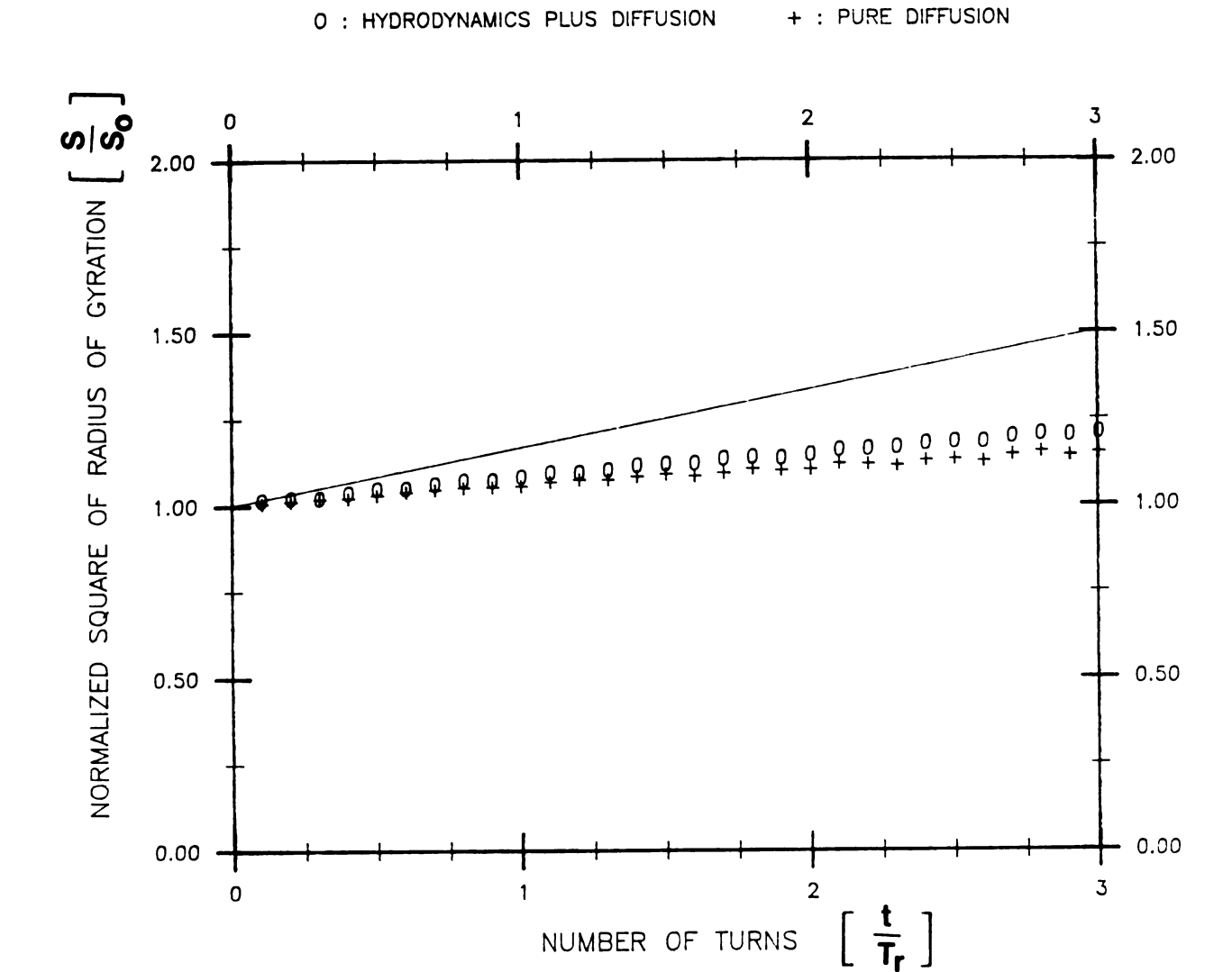


Figure 3.10 Time-Dependent Radius of Gyration Calculated Using N=6 per Lobe for Pure Diffusion and Hydrodynamic Motion with Diffusion. The Straight Line is the Theoretical Solution Given by Equation (25)



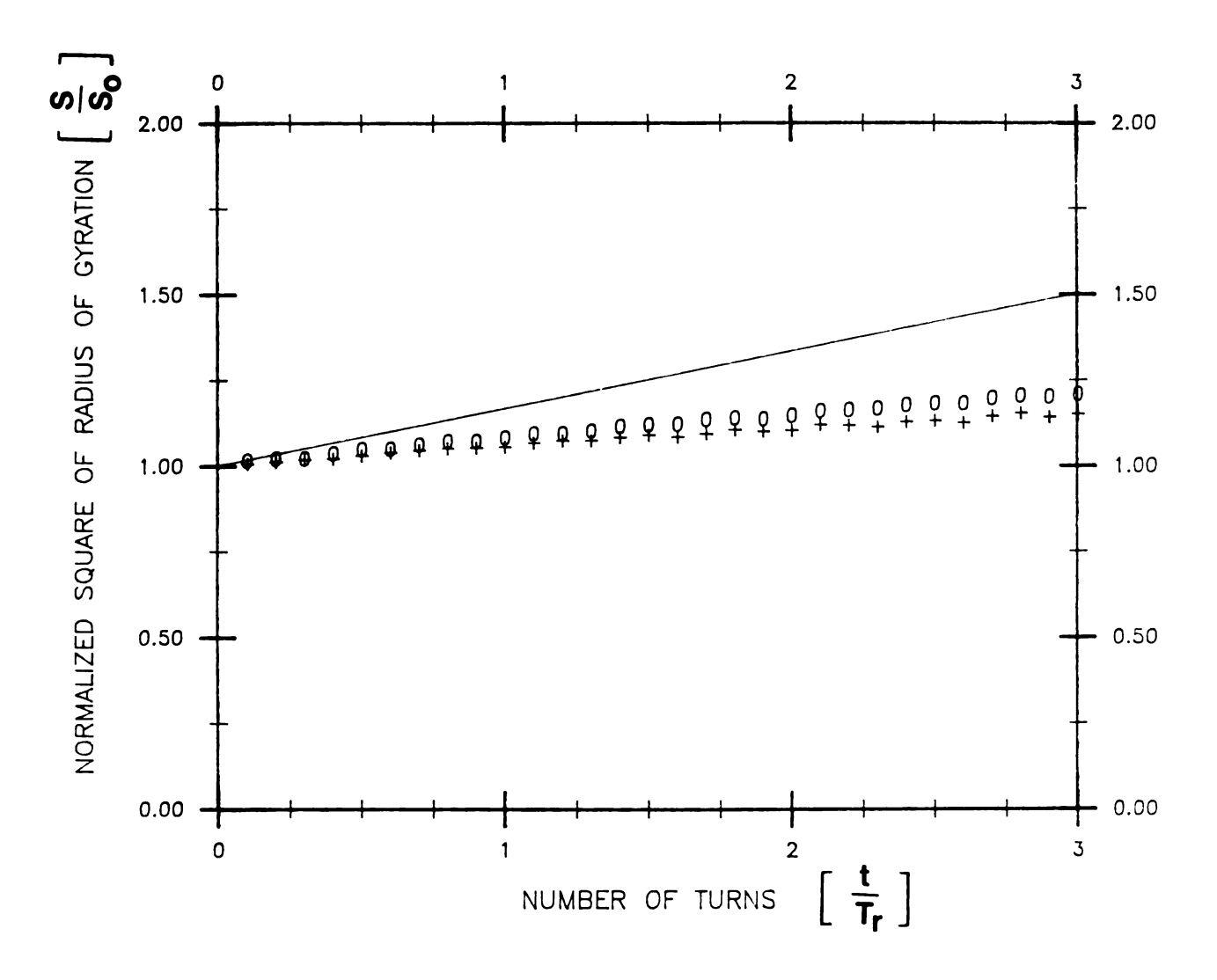


Figure 3.10 Time-Dependent Radius of Gyration Calculated Using N=6 per Lobe for Pure Diffusion and Hydrodynamic Motion with Diffusion. The Straight Line is the Theoretical Solution Given by Equation (25)



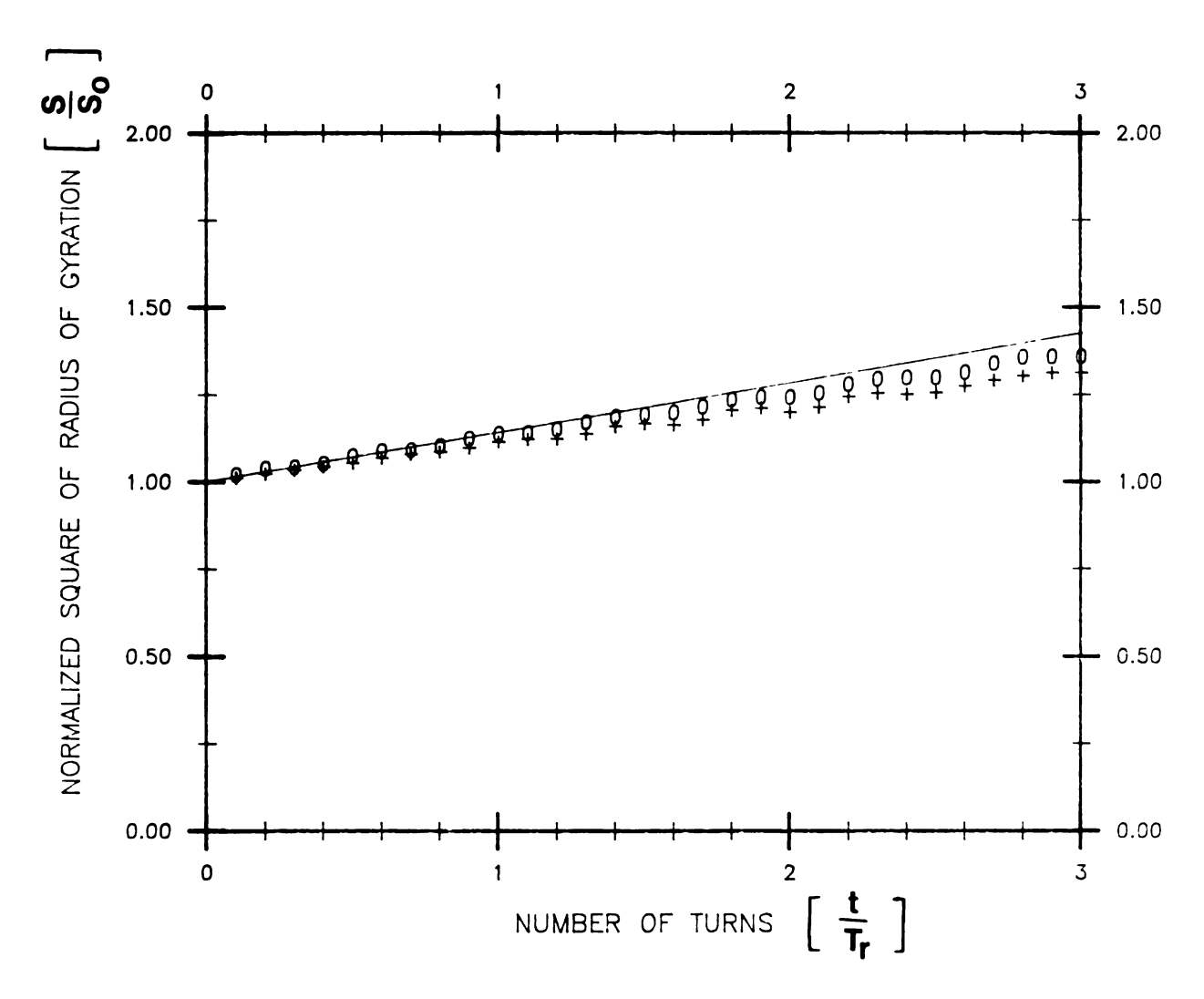


Figure 3.11 Time-Dependent Radius of Gyration Calculated Using N=60 per Lobe for Pure Diffusion and Hydrodynamic Motion with Diffusion. The Straight Line is the Theoretical Solution Given by Equation (25)



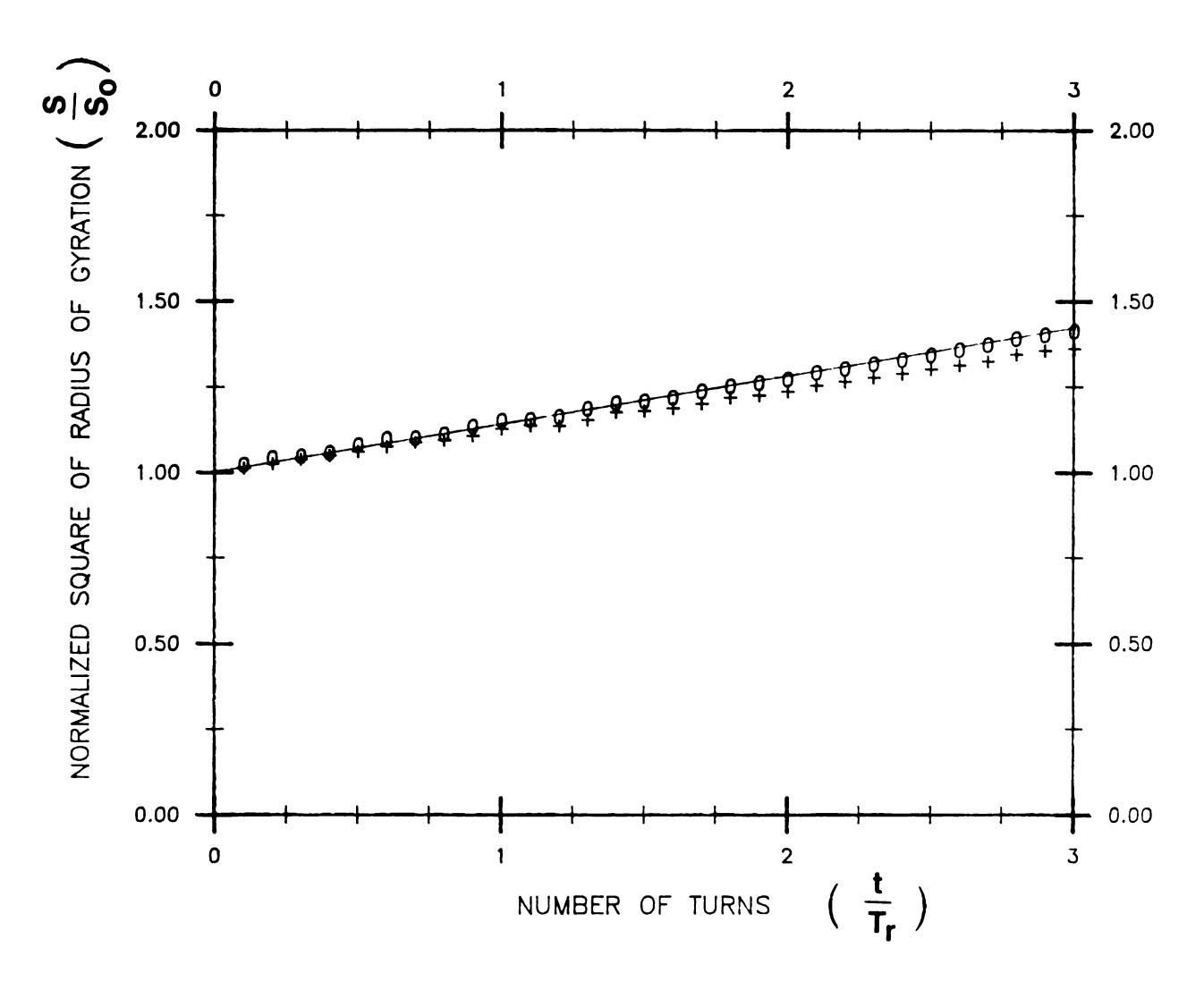
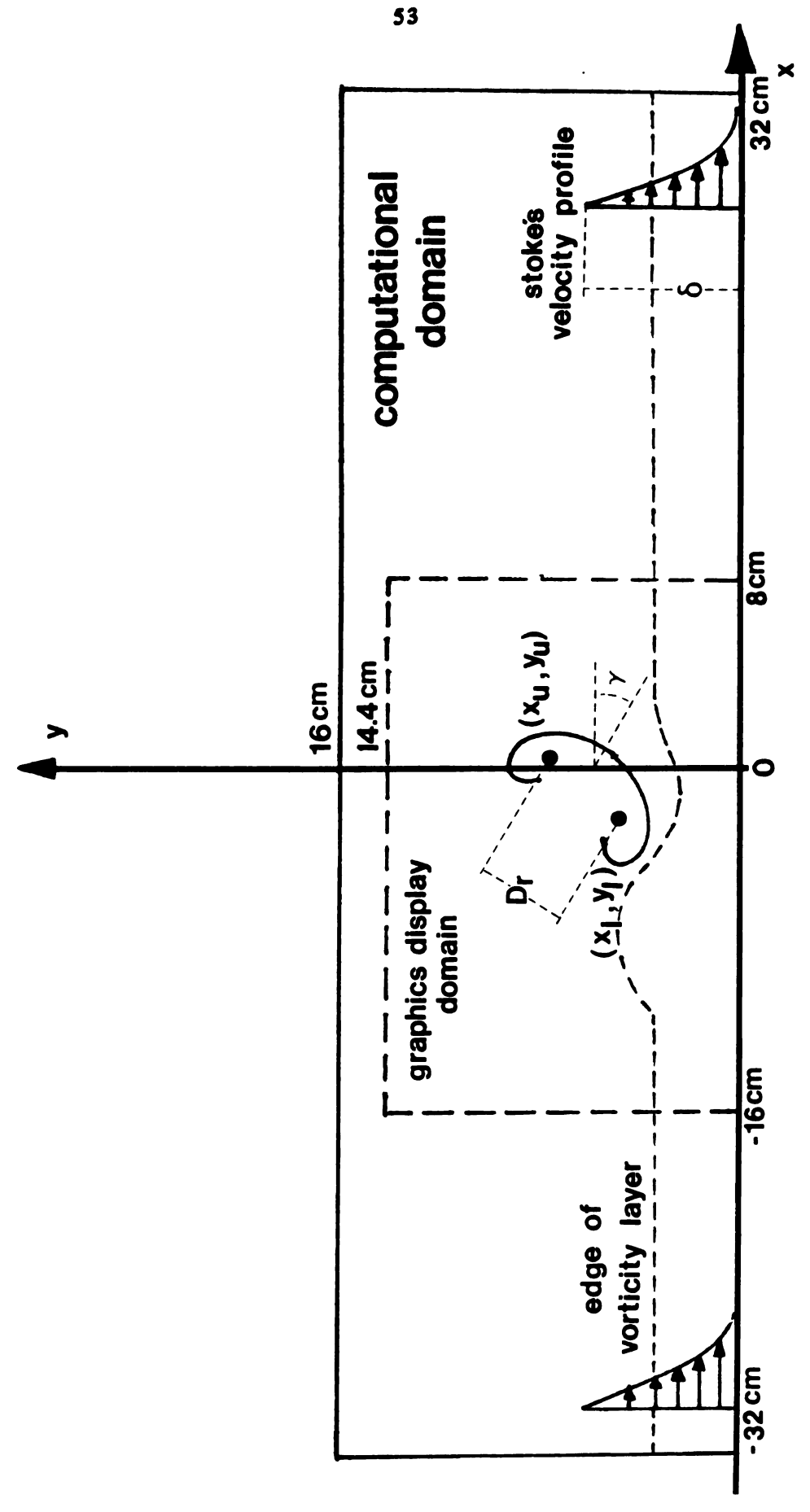


Figure 3.12 Time-Dependent Radius of Gyration Calculated Using N=500 per Lobe for Pure Diffusion and Hydrodynamic Motion with Diffusion. The Straight Line is the Theoretical Solution Given by Equation (25)



The Geometrical Arrangement of Vortex Ring/Moving Wall Interactions for Vortex-In-Cell Numerical Simulations Figure 3.13

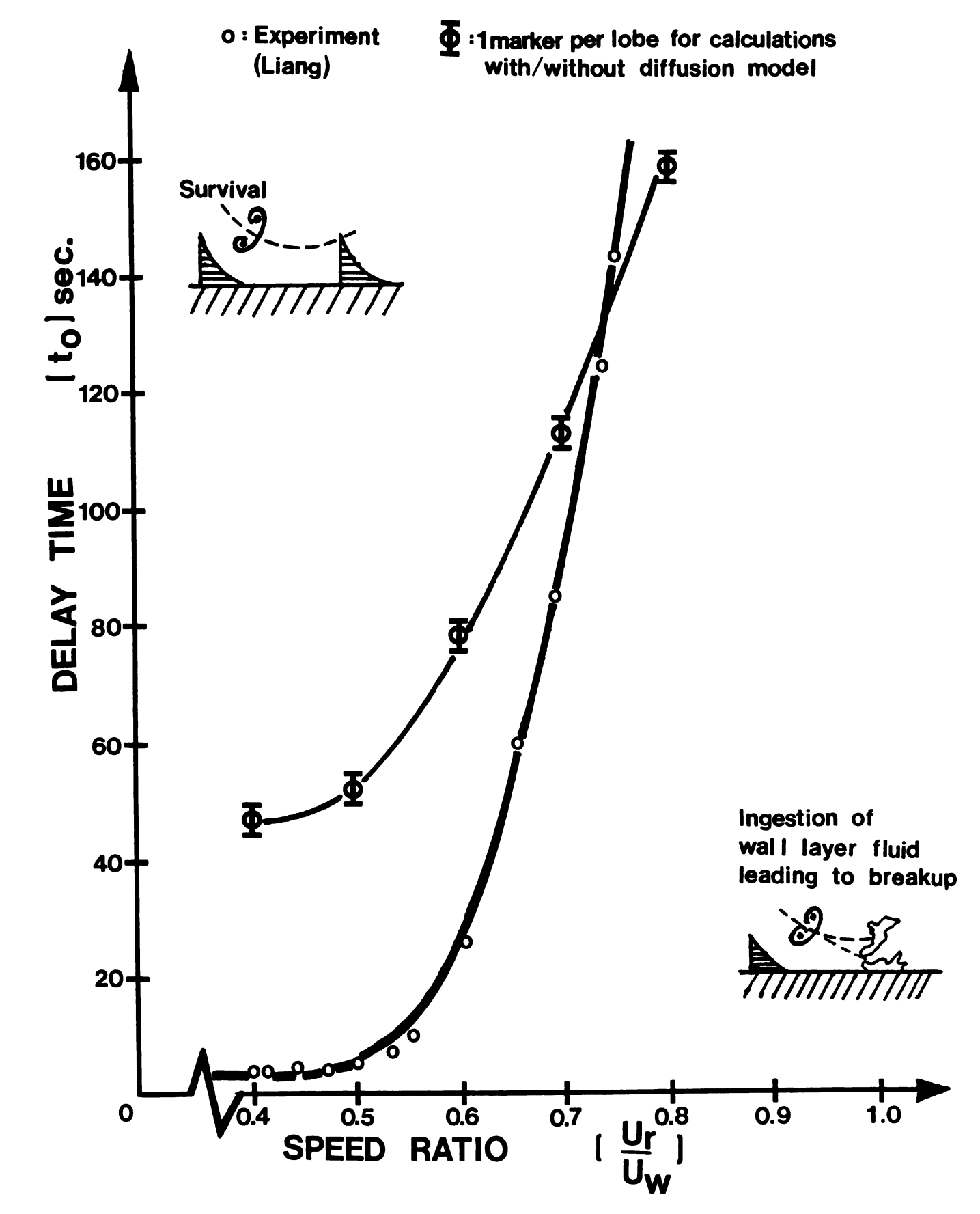


Figure 4.1 Stability Maps of Computations with/without Diffusion Model for  $\gamma=15^{\circ}$  Compared with Experimental Result of Liang[1984]. The Error Bars for Calculated Outcomes are  $\pm 2.5$  sec.

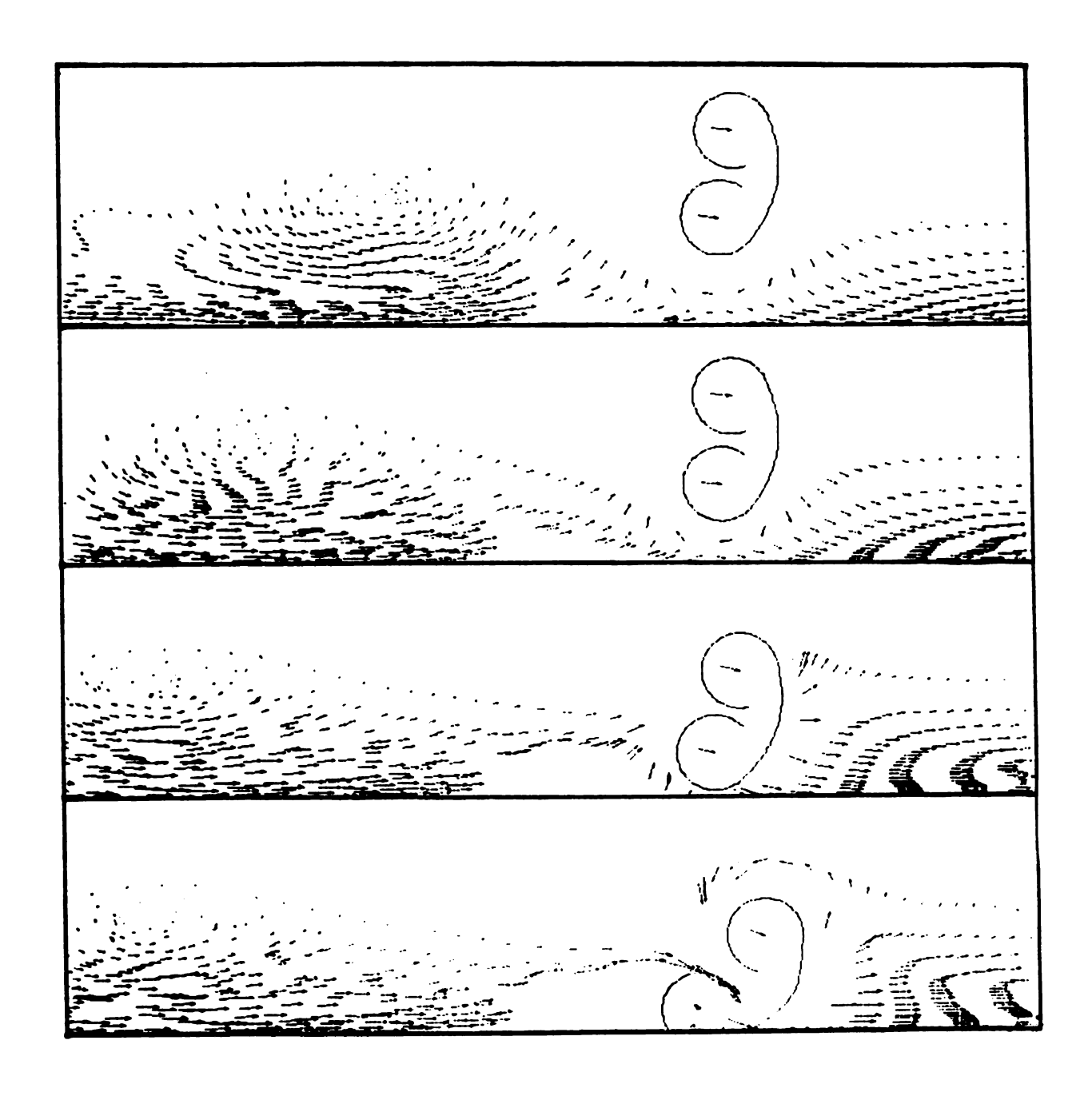


Figure 4.2 Computer Generated Vorticity Motion Pictures for an Unstable Interaction which the Line Pair Ingests Wall Layer Fluid as it "Crashes" on the Wall

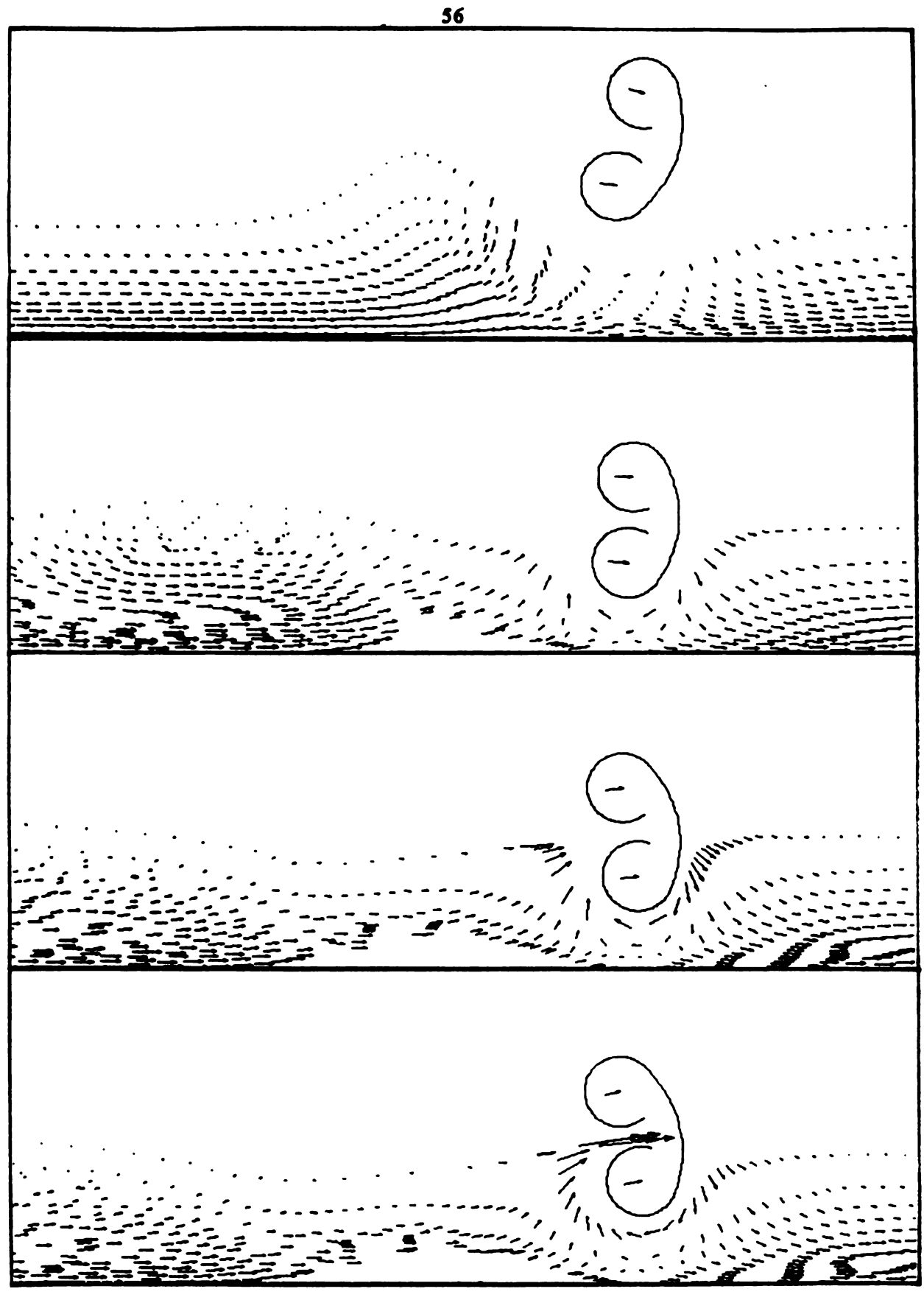


Figure 4.3 Computer Generated Vorticity Motion Pictures for an Unstable Interaction which the Line Pair Ingests Wall Layer Fluid as it Turns Away from the Wall

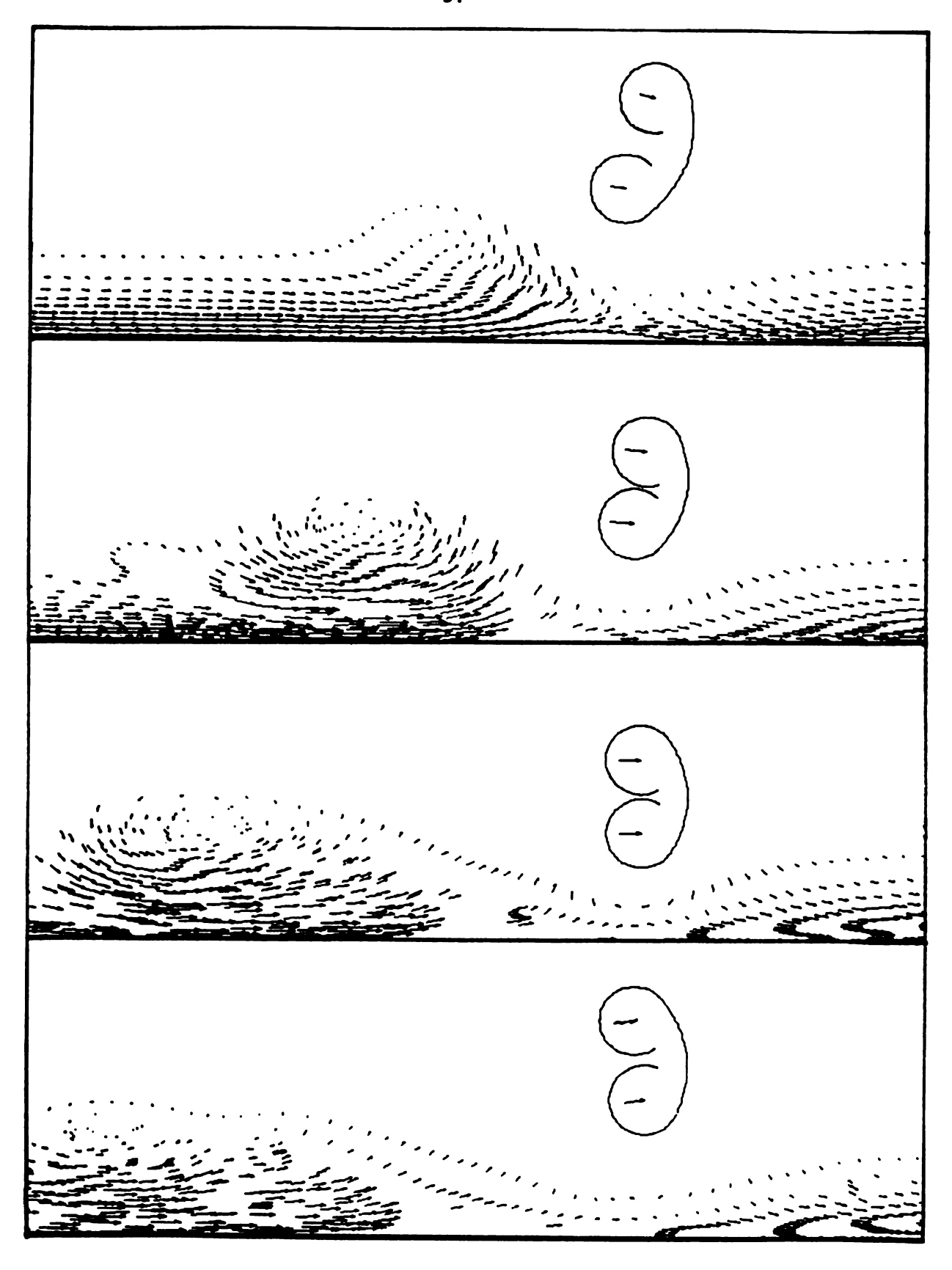


Figure 4.4 Computer Generated Vorticity Motion Pictures for a Stable Interaction which the Line Pair Leaves the Wall without Breaking Up

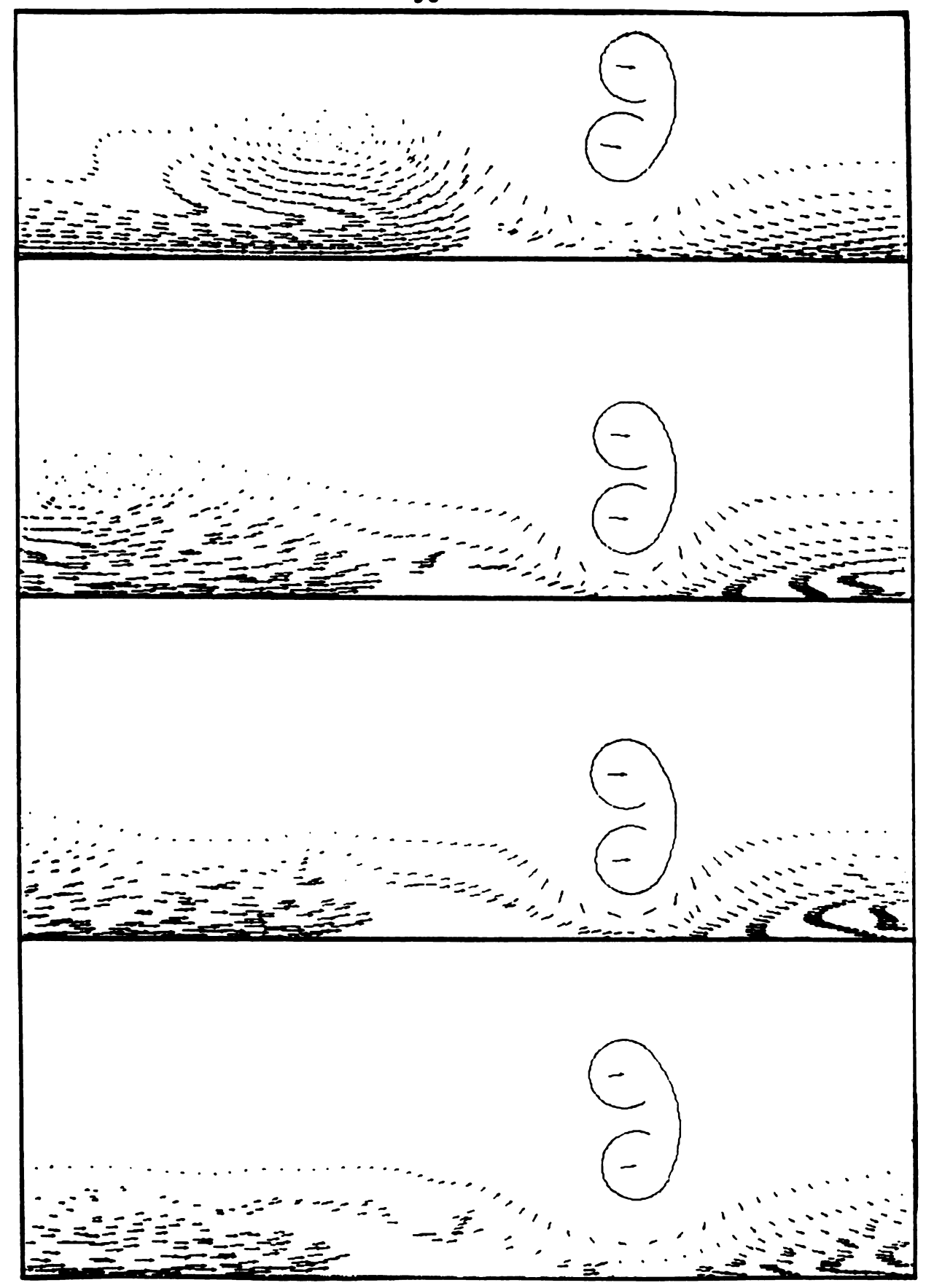


Figure 4.5 Computer Generated Vorticity Motion Pictures for a Stable Interaction in the Absence of Diffusion Process. "Photos" Correspond to The Same Time Step Number as Figure 4.6 Which The Initial Conditions Were Set Identically to This Case

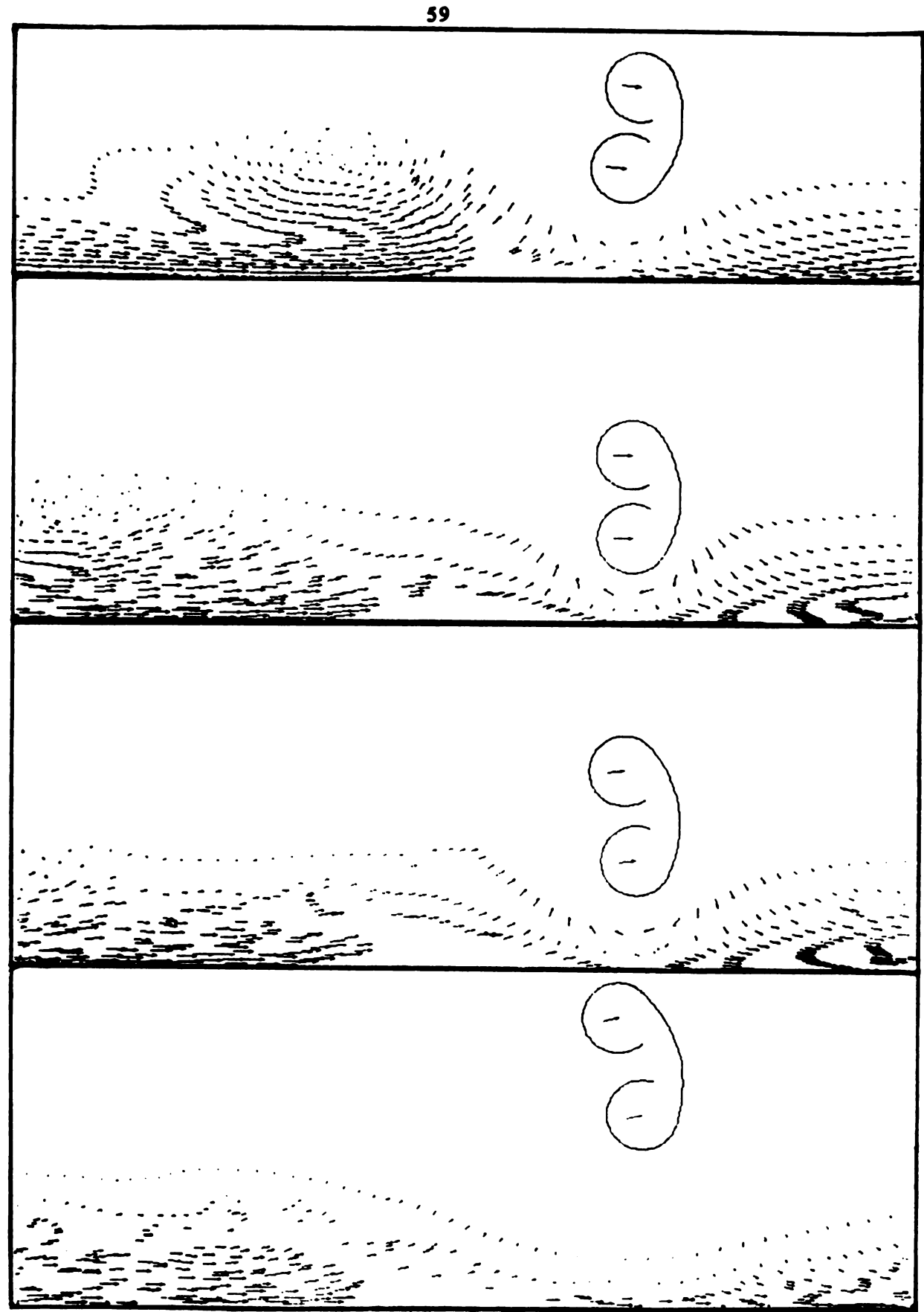


Figure 4.6 Computer Generated Vorticity Motion Pictures for a Stable Interaction in the Presence of Diffusion Process. "Photos" Correspond to The Same Time Step Number as Figure 4.5 Which The Initial Conditions Were Set Identically to This Case

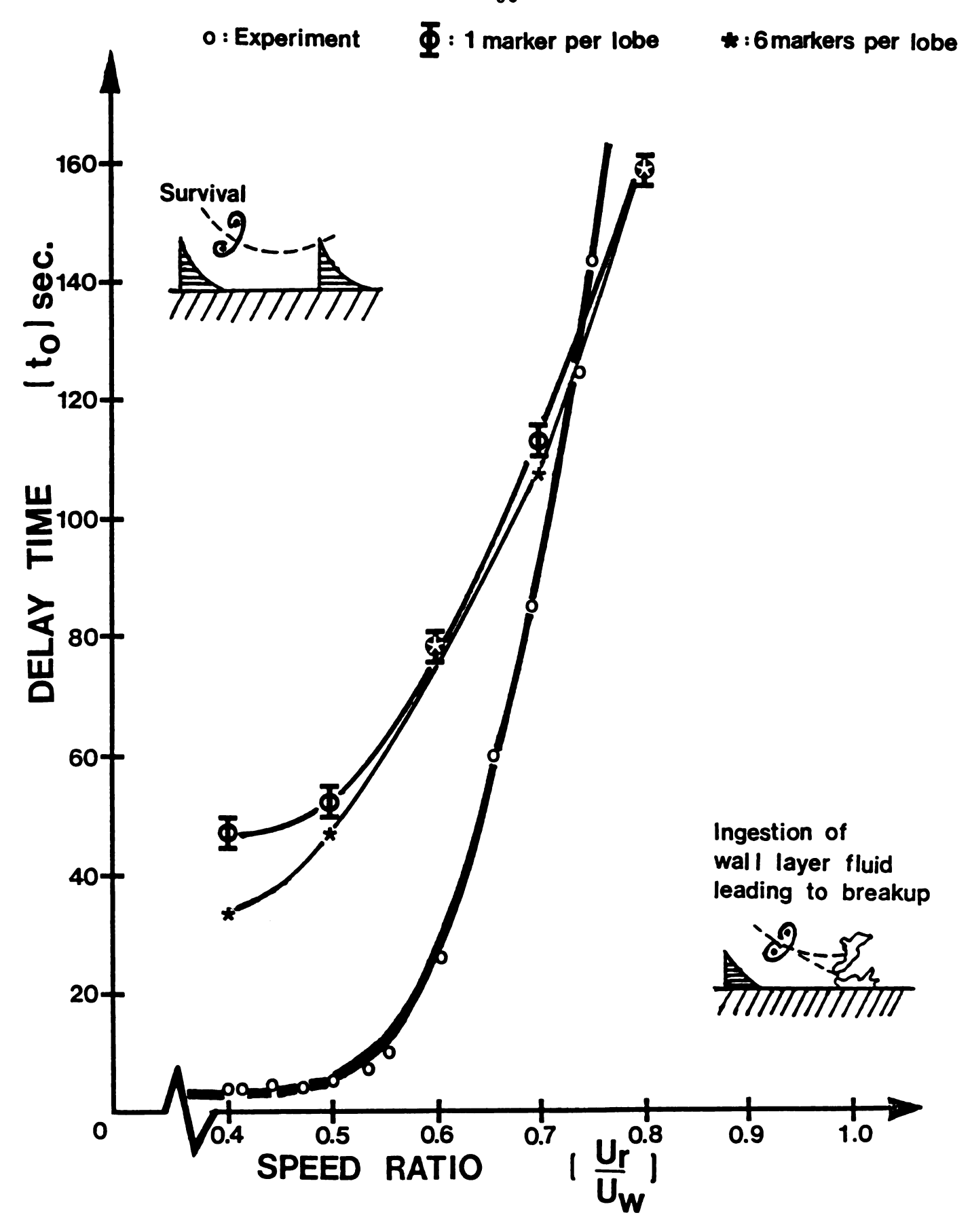


Figure 5.1 Comparisons of Stability Maps for  $\gamma=15^{\circ}$ . Calculations without Diffusion for 6 Markers per Lobe were Carried Out by Bartholomew